Renewable and Sustainable Energy Reviews 178 (2023) 113233

Contents lists available at ScienceDirect

Renewable and Sustainable Energy Reviews

journal homepage: www.elsevier.com/locate/rser

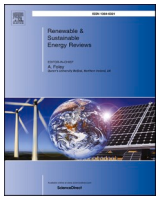

Experimental validation of a solar system based on hybrid photovoltaic-thermal collectors and a reversible heat pump for the energy provision in non-residential buildings

M. Herrando [a,*], A. Coca-Ortegón [b], I. Guedea [b], N. Fueyo [a]

[a] Fluid Dynamics Technology Group, I3A, University of Zaragoza, Zaragoza, 50018, Spain
[b] ENDEF Solar Solutions, Zaragoza, 50820, Spain

ARTICLE INFO

Keywords:
Hybrid photovoltaic-thermal (PV-T) collector
Experimental validation
Reversible heat pump
Monitoring system
Transient model
Space cooling
Space heating

ABSTRACT

This work aims to validate a transient model of a solar hybrid pilot plant based on photovoltaic-thermal (PV-T) collectors integrated via thermal storage tanks with an air-to-water reversible heat pump (rev-HP). The pilot plant is in operation and provides space heating, cooling, domestic hot water (DHW) and electricity to an industrial building located in Zaragoza (Spain). The plant consists of eight uncovered PV-T collectors (2.6 kW_e, 13.6 m^2), two water tanks and a rev-HP with a nominal thermal power of 16 kW for heating and 10.5 kW for cooling. The validation results show that the transient model fits the experimental performance of the PV-T collectors, with an average error of -16% and 3%, for the thermal and electrical generation respectively. The accuracy of the estimated rev-HP performance depends on the operation mode. The estimated COP in cooling mode has an average error of 14%, while in heating mode has an average error of -10%. The results show that the integration of the thermal and electrical generation of the PV-T collectors with a high-performance rev-HP allows the solar PV-T system to be self-sufficient to satisfy the building energy demand.

1. Introduction

Heating and cooling (H/C) account for half of the EU energy consumption (983 Mtoe in 2019) [1]. The energy demand is mainly for space heating (52%) process heating (30%) and water heating (10%), while space cooling demand is currently low but it is rapidly increasing [2]. Heating and cooling are mainly consumed in the residential sector (45%), industry (37%) and services (18%) [3]. However, H/C demands in buildings are mainly satisfied by fossil fuel technologies [4], while renewable energy sources (RES) only contributed 22% to the H/C consumption in 2019 [1]. Thus, the development and implementation of RES for building H/C are essential to increase the share of RES and therefore displace fossil-fuel utilization, reducing its associated greenhouse gas emissions [5]. Solar heating and cooling (SHC) technologies appear as an attractive solution [6], but further investment in existing and future solar technologies is necessary to reduce the costs and make these systems cost-competitive [7], as well as to ensure appropriate infrastructure [8].

Most of the published research focuses on SHC technologies that use solar thermal collectors [9] for solar cooling [10], with more than 1200 installations reported around the world [11]. Both air- and liquid-based solar thermal collectors have been coupled with an air-air or a water-water heat pump (HP) respectively [12]. The integration of solar thermal collectors with an HP takes advantage of the higher source temperature of the collectors to enhance the HP performance [13]. Alternatively, photovoltaic (PV) panels can be integrated into solar-assisted heat pump (SAHP) systems for solar heating [14] and solar cooling [15]. However, the generation and consumption profiles of PV and HP respectively are usually barely coupled and need to be integrally managed [16].

As distributed solar generation becomes increasingly deployed in urban environments, the amount of suitable space for solar installations will be increasingly scarce [17]. In this context, hybrid photovoltaic-thermal (PV-T) collectors combine the output of PV and solar thermal systems from the same aperture area [18], generating simultaneously electricity and useful heat [19], with higher overall efficiency than the separate systems [20]. In addition, PV-T collectors integrated with H/C technologies allow the simultaneous generation of hot water, cooling and electricity [21], and thus have the potential to cover a significant fraction of the energy demands of buildings [22].

Previous studies integrated concentrated PV-T collectors with H/C

* Corresponding author.
E-mail address: mherrando@unizar.es (M. Herrando).

https://doi.org/10.1016/j.rser.2023.113233
Received 29 December 2021; Received in revised form 19 January 2023; Accepted 6 March 2023
Available online 16 March 2023

Nomenclature

A_{PVT}	PV-T collector area [m^2]
β	Power temperature coefficient [%/K]
COP	Coefficient of performance [−]
c_p	specific heat capacity [J/kg K]
Δt	time step [h]
ΔT	*t*emperature difference [°C]
E_{HP}	HP electricity consumption [kWh]
E_{PVT}	PV-T electricity yield [kWh]
G_g	Incident global solar irradiance [W/m^2]
$\dot{m}_{PVT}$	Mass flow-rate in the PV-T circuit [kg/h]
η_e	Electrical efficiency [%]
$\eta_{e,ref}$	Electrical efficiency at reference conditions [%]
η_{th}	Thermal efficiency [%]
p_{HP}	HP electrical power consumed [W]
p_{PVT}	PV-T electrical output [W]
T_{HPin}	HP inlet water temperature [°C]
q_{th}	PV-T useful thermal output [W]
q_{HP}	HP thermal power generated [W]
Q_{DHW}	DHW demand [kWh]
$Q_{heating}$	Heating demand [kWh]
Q_{HP}	HP thermal energy generated [kWh]
Q_{PVT}	PV-T thermal energy yield [kWh]
SCF_{eHP}	Electrical solar contribution factor to the HP [−]
SCF_{th}	Thermal solar contribution factor [−]
T_a	Ambient temperature [°C]
T_{cell}	PV cell temperature [°C]
T_{DHW}	DHW supply temperature [°C]
T_m	Average water temperature [°C]
T_{HPin}	HP inlet water temperature [°C]
T_{PVTin}	PV-T inlet water temperature [°C]
T_{PVTout}	PV-T outlet water temperature [°C]
T_{PVToT}	PV-T outlet water temperature at the tank entrance [°C]
T_{tBot}	Tank temperature at the bottom [°C]
u'	Reduced wind speed [m/s]
u_w	Wind speed [m/s]

Abbreviations

DHW	Domestic hot water
H/C	Heating and cooling
HP	Heat pump
PID	Proportional–integral–derivative
PV	Photovoltaic
PV-T	Photovoltaic-thermal
RES	Renewable energy sources
rev-HP	Reversible heat pump
SAHP	Solar assisted heat pump
S–CCHP	Solar combined cooling heating and power
SHC	Solar heating and cooling

technologies [23]. For instance, parabolic dish concentrated PV-T collectors using triple-junction PV panels were integrated with double-effect LiBr–H_2O absorption chillers to provide electricity, space heating, cooling and DHW to buildings [24]. The simulation results showed thermal efficiencies of ~60% over a wide range of operating conditions along with 19–25% electrical efficiencies [25]. In addition, nanofluids have been proposed in concentrated PV-T collectors for the provision of heating and cooling [26], concluding that, in the long-term, the nanofluid-based system is preferred to a water-based system.

The integration of water-based PV-T collectors with LiBr–H_2O absorption chillers showed an important energy-saving potential in buildings thanks to the provision of heating, cooling and electricity [27]. The results show that the highest solar utilization factor (of 0.24) is achieved with covered PV-T collectors while the shortest payback time is achieved with uncovered PV-T collectors [28]. An auxiliary heater is always required to satisfy the energy demands when there is not enough solar irradiance as well as to ensure a safe system operation [29]. However, the economics of these systems considerably depend on the utility prices of the specific application [30], requiring in most cases public funding or economic incentives to be cost-competitive with conventional alternatives [31]. Previous research concluded that water-based PV-T collectors integrated with H/C technologies can cover more than half of the space heating, domestic hot water (DHW) and cooling demands of households [32].

A recent review concluded that the integration of PV-T collectors with HPs is an important research area as it has the potential of cogenerating heat and electricity with improved overall efficiency and reliability [33].

Some authors analysed air-based PV-T collectors coupled with HPs [34]. The modelling results [35] of a system where an air-source HP uses the warm air generated in the air-based BIPV-T collector for space heating provision in residential households showed that the proposed system was a highly efficient heating system in winter conditions, and concluded that there is an important electricity cost reduction potential. In this line, an experimental analysis [36] of an air-based PV-T collector integrated with an air-to-water HP showed a COP enhancement of 3.1% (average) and 8.6% (maximum) compared to an air-source HP. Theoretical works of a PV-T double façade system for space heating showed electrical efficiencies of 8–11% in New Delhi (India) [37], while site-scale experimental works in Busan (South Korea) obtained an average electrical efficiency of 17%, an average thermal efficiency of 38%, and an average HP COP of 3.4 [38]. This integration seems interesting in applications where water is in limited supply [38], but it has limitations due to the low density and small heat capacity of air.

Alternatively, several authors [39] proposed the integration of refrigerant-based PV-T collectors with HPs, where the PV-T collector acts as the HP evaporator [40] to provide space or water heating [41], enhancing the COP of the HP [42]. There are several theoretical studies [2] focused on direct expansion SAHP systems that provide heating to buildings. The reported thermal efficiencies of the PV-T collectors vary from 32% [43] to 55% [44], while electrical efficiencies are between 12% [45] to 19% [44]. The simulation results of another study [45] showed a year-averaged COP of 5.9 and an electrical efficiency of 12%, concluding that the energy output of a PV-T SAHP system is higher than that of a conventional side-by-side PV and HP system. In this line, other authors obtained an average COP of 6 in a PV-T SAHP system operating with a variable-frequency compressor [46]. Previous authors [47] also showed promising results for a solar system based on PV-T collectors and an HP with a variable speed compressor to provide the heating demand in winter in Nanjing and Hong Kong (China). Recent theoretical research [48] proposed the integration of refrigerant-based PV-T collectors with a reversible HP (rev-HP) to provide electricity, heating and cooling. The PV-T collectors produced cooling at night-time by longwave radiation exchange with the sky and convection losses to the ambient air.

There are also some experimental works at the laboratory scale reported in the literature [49]. A direct expansion SAHP system that provides heating was experimentally tested on a rig [50], obtaining an average COP of 5.4, with a PV-T electrical efficiency of 13%. A prototype of a refrigerant-based PV-T collector acting as the evaporator of an HP was experimentally tested, showing an improvement in the electrical efficiency of 15% compared to a conventional PV module and an average system COP of 3.91 [51]. A glass vacuum tube PV-T collector with a U-shape copper tube as an evaporator and amorphous silicon PV cells integrated with an HP was experimentally tested in Nottingham

[52]. The results showed an average COP between 3.8 and 4.3 depending on the solar irradiance, condenser water temperature and water flow rate.

More recently, other authors [53] analysed the performance of a roll-bond PV-T collector acting as the evaporator in heating mode [54] and as the condenser in refrigeration mode [55] of a single-stage compression HP in northern China. The experimental results showed an average daily system COP of 4.7 for heating under real testing conditions [56]. In cooling mode, the experimental COP varied from 2.4 to 3.5 with an average value of 2.8 during the chilled water process, and from 1.9 to 2.9 with an average value of 2.3 during the ice process [55]. There are also promising economic analyses of refrigerant-based PV-T collectors integrated with HPs, showing payback times of less than 5 years [57].

Recently, experimental research on an opaque ventilated PV-T system integrated with an HP was presented [58]. The PV-T façade was used as the evaporator of the HP while generating electricity, and at the same time, the cavity preheated the fresh air of the building. The experimental results showed a maximum COP of 3.1 and an average electrical efficiency of 9% during the testing period.

Heat-pipe PV-T collectors have also been integrated with an HP for domestic heating [59], showing PV-T efficiencies of 40% (thermal) and 10% (electrical). The economic analysis performed concluded that local utility prices and renewable incentives are critical for the financial feasibility of these systems [60].

Water-based PV-T collectors can also be integrated with rev-HPs [32], using the PV-T thermal output in the heating mode to increase the COP [61], while in both heating and cooling modes, the PV-T electrical output can be used to run the HP [62]. Most of the studies found in the literature are theoretical [2].

Previous authors [63] proposed the integration of water-based PV-T collectors with a water-to-water HP for the provision of space heating and electricity to households [64], concluding that high flow rates and larger storage tanks enhance the total PV-T collector efficiency [43]. Recent research [65] analysed different control strategies in this type of system. In this line, a polygeneration system was proposed by some authors [66] in which the hot water generated by the PV-T collectors was used in winter in the HP evaporator to provide space heating, while in summer it was used to run an adsorption chiller to provide space cooling.

The experimental results of PV-T collectors with a micro-channel heat absorber integrated with a water-source HP are also promising [67], showing a COP in heating operation mode from 3.2 [68] to 4.9 [69], and PV-T efficiencies of 32% [69] to 38% (thermal) [68] and 14% (electrical) [69]. In this line, a theoretical model of water-based PV-T collectors (fractal shape) integrated with a water-source HP for water heating in sports centres showed an average COP of 4.2, and a payback time of 10.5 years when the system is located in Hong Kong [70]. Other experimental analyses [71] showed that uninsulated PV-T collectors can work to directly heat water in sunny periods and as a heat exchanger with the ambient in periods with solar irradiance below 50 W/m^2, connected to the source of a brine-water HP, which can provide the hot water.

Alternatively, other authors [72] proposed the integration of roll-bond PV-T collectors with a dual-source air-to-water rev-HP, developed a transient model for the system and compared the results with a PV SAHP system. The comparison of four alternative SAHP heating systems concluded that the integration of PV-T collectors with a water-source HP seems the best alternative in locations with high electricity prices [73].

Air-source HPs can also be integrated with water-based PV-T collectors in dual indirect systems [74], with the PV-T collector operating as the evaporator in parallel with the air-source HP evaporator [75]. The air-source evaporator can recover heat under low radiation levels, while the PV-T evaporator can compensate for the performance degradation of the air-source evaporator caused by the increasing condensing temperature [74].

There is a considerable number of theoretical analyses on PV-T collectors integrated with HPs, particularly using refrigerant-based PV-T collectors [57]. Meanwhile, most of the current PV-T manufacturers focus on water-based PV-T collectors [76] and 57% of the total installed PV-T thermal capacity corresponds to uncovered water-based PV-T collectors [77]. These facts show that this type of PV-T collector is gaining attention in the market, although more applied research is still needed in the integration of water-based PV-T collectors with HVAC technologies, as highlighted in Task 60 of the International Energy Agency [78].

The majority of previous studies are based on theoretical models [48], some of which are validated with experimental results from literature or test rigs [79]. There are also some experimental works, although, usually, the systems are small-scale (e.g. a couple of PV-T collectors and an HP) [80], and tested in a rig under controlled operating conditions or during some days in a specific season (e.g winter or summer conditions). Most of the findings of previous research show that PV-T SAHP systems have an important potential to decarbonise the building [81] and industry [82] sectors, even in climates with low irradiance levels or in countries with a highly decarbonised electricity supply [81].

Still, experimental and validation studies of a full-size solar system installed in a building under real operating conditions, such as the one proposed in this work, are scarce [83]. For instance, a recent review [84] concluded that there is a lack of demonstration studies of PV-T systems in real buildings.

The present research addresses this gap by considering a full-size pilot plant located in Spain and operating under real weather conditions (in winter, spring and summer seasons). This solar hybrid pilot plant consists of water-based PV-T collectors integrated with an air-to-water rev-HP via thermal storage tanks. It provides space heating, cooling, DHW and electricity to an industrial building, which consists of an office area, and an assembly area. Unlike many other previous works, which use data from test rigs or from the literature for validation, real monitoring data provided by the plant is used in this work, together with actual energy demands. This is one novelty of this research.

Additionally, the literature also shows a lack of studies of the solar-assisted heat pump system proposed in this work, *viz* water-based PV-T collectors integrated with a reversible air-to-water heat pump for the provision of heating, cooling and electricity. This is one of the original contributions of this work. Most of the solar PV-T systems have been integrated into residential buildings [85], and some in fitness centres [70], universities [21] and offices [61]. Meanwhile, the application in industrial buildings is less common, which is another novelty.

2. Materials and methods

The solar hybrid pilot plant consists of eight uncovered PV-T collectors (2.6 kW$_e$, 13.6 m^2), two water storage tanks (of 350 l for DHW and of 263 l for space heating/cooling) and an air-to-water rev-HP. The space heating/cooling distribution circuit uses fan coils as terminal units, allowing a minimum supply temperature of 35 °C in winter and 7 °C in summer. To increase the use of low-temperature heat, DHW is supplied at 50 °C instead of 60 °C, performing periodic heat treatments at 60 °C to avoid legionellosis according to sanitary regulations [86].

The pilot plant has been in operation under real conditions from February 8th until August 25^{th,} 2021 with some idle periods to implement performance changes or to perform maintenance. Detailed results of the experimental performance can be found in previous work [87]. Section 2.1 summarises the main components of the pilot plant; Section 2.2 details how the different components are modelled in the software, and Section 2.3 summarises the key performance indicators analysed to validate the transient model.

2.1. Solar hybrid pilot plant

In the solar hybrid pilot plant, the PV-T thermal output is used to heat the water of two parallel storage tanks (see Fig. 1), one (the hot-water tank) for DHW, and the other (the inertia tank) for space heating in winter and space cooling in summer. In both heating and cooling modes, as well as for DHW production, the rev-HP acts as an auxiliary heater/cooler to reach the set-point temperatures of the building's thermal demand. The rev-HP is electrically powered by the PV-T collectors, and the PV-T electrical output not consumed by the rev-HP is used to match the building electricity demand (for lighting and other electrical devices).

2.1.1. PV-T collectors

The PV-T field consists of eight PV-T collectors, these prototypes were manufactured by ENDEF [88], and arranged in parallel. The PV-T collectors are unglazed, with a sheet-and-tube spiral heat exchanger, a nominal electrical power of 320 W_p and a gross area of 1.70 m^2 (see Fig. 2). The PV-T parameters are detailed in Table 1.

Previous experimental analyses in a test bench under controlled operating conditions following the requirements of the ISO 9806:2017 standard [89] allowed the estimation of the thermal performance curve (q_{th}, in W/m^2), as follows:

$$q_{th} = \eta_0 G_g - a_1(T_m - T_a) - a_2(T_m - T_a)^2 - a_3 u'(T_m - T_a) + a_4\left(E_L - \sigma T_a^4\right) - a_5\frac{dT_m}{dt} - a_6 u' G_g - a_7 u'\left(E_L - \sigma T_a^4\right) \quad (1)$$

where u' is the reduced wind speed (estimated as u_w - 3 m/s), T_m is the average water temperature, T_a is the ambient temperature, G_g is the global solar irradiance [89]. The PV-T collector parameters were obtained following a multivariable fit approach using experimental data obtained in the test bench (see Table 1) [89].

2.1.2. Reversible air-to-water heat pump

The reversible air-to-water HP selected for this research is the Yutaki S6 model, manufactured by Hitachi [90]. The main heat pump parameters are detailed in Table 2. Water can be provided from 20 °C to 60 °C in heating mode, from 30 °C to 60 °C for DHW production, and from 5 °C to 22 °C in cooling mode.

2.1.3. Water storage tanks

The hot-water tank from Lapesa [91] has a capacity of 350 l and two internal heat exchangers, one for the solar circuit (in the lower part) and the other one for the rev-HP unit (in the upper part). Coldwater from the mains enters at the bottom and leaves from the top for DHW. The inertia tank from Greenheiss [92] has a capacity of 263 l and one internal heat exchanger for the solar circuit, covering approximately 2/3rd of the tank height. The HP circuit enters and exits at the upper part, while the heating/cooling circuit enters at the bottom and leaves from the upper part of the tank.

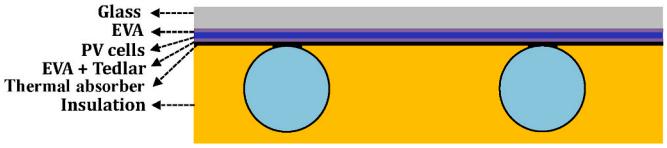

Fig. 2. Schematic diagram of the PV-T collector (not to scale).

Table 1
PV-T collector parameters.

PV-T collector parameter			Value
Nominal electrical power			320 W_p
Gross area			1.70 m^2
Electrical efficiency at reference conditions[a] **($\eta_{e,ref}$)**			18.8%
Power temperature coefficient (β)			0.37 %/K
PV-T collector parameters (ISO 9806:2017 standard)			
η_0	0.344	a_4	23,530
a_1	9.60	a_5	0.279
a_2	0	a_6	0.0089
a_3	0.0128	a_7	0

[a] Reference conditions: 25 °C and 1000 W/m^2.

2.1.4. Monitoring system

The thermal performance of the pilot plant is monitored through temperature sensors and flow meters (see Table 3) installed in the hydraulic circuits (marked in different colours in Fig. 1): solar circuit, HP circuit, DHW circuit and heating/cooling circuit. The electricity generated by the PV-T collectors is monitored through a DC/AC inverter integrated into the overall monitoring system, and the electricity consumed by the rev-HP is also measured and fed into the monitoring system. The weather data monitored include ambient temperature (T_a), global solar irradiance at the collector slope (G_g) and wind speed (u_w). All the variables are monitored every minute.

The measurement uncertainties of the main pilot-plant variables are estimated considering the accuracy of the different sensors indicated in

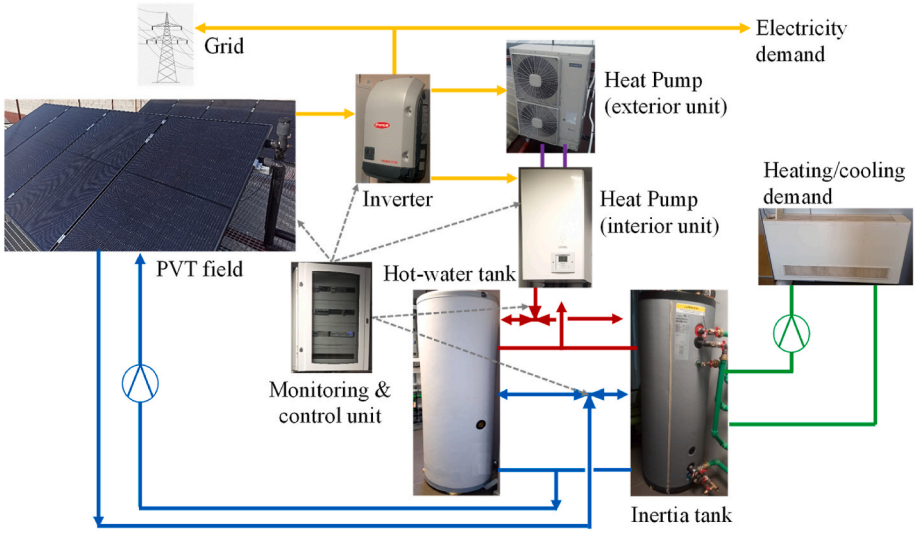

Fig. 1. Schematic diagram of the solar hybrid pilot plant including the main components.

Table 2
Air-to-water heat pump parameters.

Air-to-water heat pump parameter	Value
Nominal capacity in heating mode[a]	16.0 kW
Nominal COP in heating mode[a]	4.57
Seasonal COP at 35 °C (SCOP)	3.90
Seasonal COP at 55 °C (SCOP)	3.20
Nominal capacity in cooling mode[b]	10.5 kW
Nominal COP in cooling mode[b]	3.31
Seasonal COP in cooling mode[b]	2.84

[a] Heating mode: operating at 30–35 °C in the water circuit and 7 °C ambient.
[b] Cooling mode: operating at 7–12 °C in the water circuit and 35 °C ambient.

Table 3. Table 4 shows that the estimated relative error for the thermal and electrical efficiencies of the PV-T collectors is below 1%.

2.2. Transient model

The solar hybrid pilot plant was previously modelled in the transient simulation software, TRNSYS [93], to size and optimise the system [22]. The main system components (PV-T collectors, rev-HP, and storage tanks) were implemented in the model by modifying the corresponding TRNSYS types to match the real characteristics and performance of the commercial units, as detailed below. Real weather data monitored in the pilot plant is integrated in the model. The transient model is run with a 5-min time-step, and the results shown in this work are averaged every hour to smooth out the results, as otherwise fluctuations obscure the graphical interpretion and comparison of results. Weekly energy results are also calculated, by integration, to compare weekly performance indicators.

2.2.1. PV-T collector

The PV-T parameters were integrated into TRNSYS Type 50 b, which uses a mathematical model based on the work of Florschuetz [94] for flat plate collectors operated at peak power and the electrical output is also solved at peak power using the I–V curves of the PV cells. The performance was checked at different wind speeds and solar irradiance levels. As shown in Fig. 3, the simulation results match the experimental performance curve within a 10% error (see error bars), for the operating temperatures (10–50 °C). Larger variations (within the 10% error) occur at lower solar irradiance (see Fig. 3 right) and high wind speeds (6 m/s).

2.2.2. Reversible air-to-water heat pump

The rev-HP is modelled using Type 941, which is based on user-supplied data files containing catalogue data for the capacity and power at different ambient temperatures and water supply temperatures [93]. The data files (performance data) are modified to fit the real performance of the unit provided by the manufacturer [90]. Specifically, the thermal capacity and power consumption of the rev-HP at different operating temperatures are compiled in the data files for both heating and cooling modes, under nominal compressor speed (3000 RPM). In heating mode, values are provided for nine water inlet temperatures (from 15 °C to 55 °C) and ten ambient temperatures (from -20 °C to 20 °C). In cooling mode, values are provided for six water inlet temperatures (from 10 °C to 27 °C) and eight ambient temperatures (from 10 °C to 45 °C). These values are normalised considering the nominal capacity in each operating mode to adapt the performance data to the type of data read by the TRNSYS Type [93].

Table 3
Summary of sensors in the monitoring system.

Sensor	Amount	Type of sensor	Technical specifications
Solar radiation sensor	1	Pyranometer thermopile type	Range: 0–2000 W/m^2, Accuracy: ± 1.2% of full scale
Wind speed sensor	1	Anemometer hemispherical cup type	Range: 0–50 m/s, Accuracy: ± 3%
Temperature sensors	28	Electronic sensor Arduino	Range: 55 to 125 °C, Accuracy: ± 0.5 °C
Flow rate sensors	4	Analogue volumetric sensor	Range: 30–3000 l/h, Accuracy ± 3% of full scale
Electrical power HP	1	Electronic power meter, integrated into the HP	Range: 0–10 kW Accuracy: ± 5%
Electrical power PV-T	1	Electronic current meter, integrated into the inverter	Range: 0–27 kW, Accuracy ± 1%

Table 4
Absolute and relative errors of the main thermal and electrical variables.

Magnitude	Unit	Absolute error	Mean value	Relative error
ΔT	°C	0.2	30	0.67%
$\dot{m}_{PVT}$	l/h	9	680	1.32%
G_g	W/m^2	20	800	2.50%
p_{PVT}	W	35	3500	1.00%
η_{th}	[−]	0.0018	0.25	0.74%
η_e	[−]	0.0004	0.16	0.26%

2.2.3. Water storage tanks

The tanks are modelled using a stratified water storage tank of constant fluid mass (Type 534) [95]; considering six fully mixed equal-volume segments along the cylinder vertical axis. The internal heat exchanger is also modelled, its cross-sectional area, coil diameter and coil pitch having been estimated from data provided by the manufacturer. The inlets and outlets to the water storage tank are modelled in segments that correspond to the real tank height.

2.2.4. Solar hybrid pilot plant

The solar hybrid plant is modelled in TRNSYS following the real layout of the pilot plant. The real weather data is an input to the model, as is the real building energy demand. The PV-T collectors are connected to the two parallel storage tanks (the hot-water tank and the inertia tank) through a diverter controlled by two ON/OFF differential controllers (Type 165). Depending on the temperature of the water leaving the PV-T collectors and the storage tank temperature, water is directed to one of the two tanks, or recirculated if it is not hot enough. The rev-HP is also connected to the two parallel storage tanks and provides heating/cooling to either of them depending on the building demand. That is, when there is DHW demand, the HP heats the upper part of the hot-water tank if it is below the DHW set-point temperature. Likewise, when there is heating or cooling demand, the HP heats or cools the inertia tank to reach the set-point temperature, if needed. Priority is given to the DHW demand, so if there are heating and DHW demands simultaneously, the HP heats first the hot-water tank to reach the DHW set-point and then it heats the inertia tank. Similarly, if there are simultaneous cooling and DHW demands, the HP heats first the hot-water tank to reach the DHW set-point and then it cools the inertia tank to provide cooling.

In summer, during the months when there is cooling demand, the PV-T circuit activates at night if the water temperature in the PV-T collectors is lower than the water in the inertia tank. In this case, the water leaving the PV-T collector cools the inertia tank (radiative cooling), so that during the day when there is cooling demand less energy is required by the rev-HP to satisfy this cooling demand.

The electricity generated by the PV-T collectors is used by the rev-HP, and the PV-T electrical output not consumed by the rev-HP is used to match the rest of the building electricity consumption (for lighting and other electrical devices).

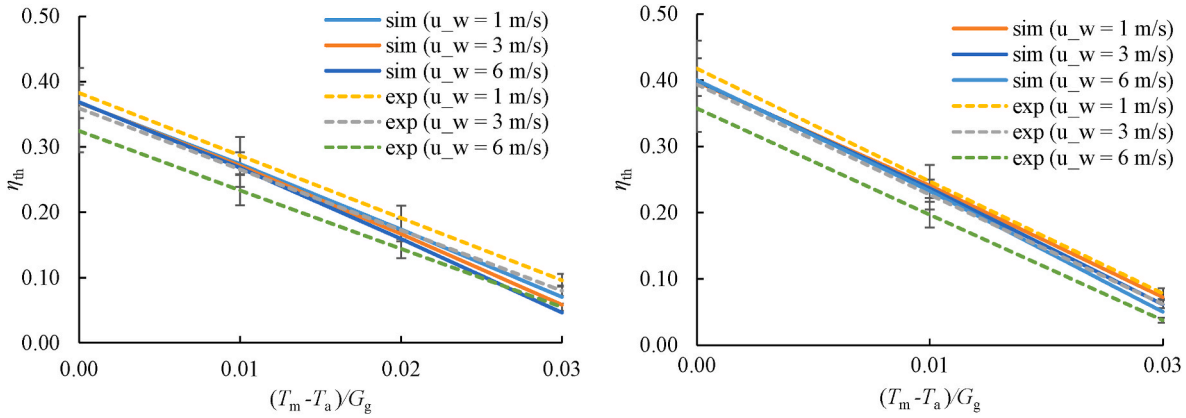

Fig. 3. Thermal performance curves of the PV-T collector from simulation (sim) and experimental (exp) data for different wind speeds (u_w) at a global solar irradiance of 1000 W/m^2 (left) and 600 W/m^2 (right).

2.3. Key performance indicators

A set of key performance indicators are defined to analyse the pilot plant and validate the model.

- Average thermal efficiency of the PV-T collectors (η_{th}):

$$\eta_{th} = \frac{q_{th}}{G_g \cdot A_{PVT}} \tag{2}$$

- Average electrical efficiency of the PV-T collectors (η_e):

$$\eta_e = \frac{p_{PVT}}{G_g \cdot A_{PVT}} \tag{3}$$

- Average COP of the rev-HP (*COP*):

$$COP = \frac{q_{HP}}{p_{HP}} \tag{4}$$

- Thermal energy yield (Q_{PVT}, kWh) of the PV-T collectors:

$$Q_{PVT} = \dot{m}_{PVT} \cdot c_p \cdot (T_{PVTout} - T_{PVTin}) \cdot \Delta t = q_{PVT} \cdot \Delta t \tag{5}$$

- Electricity yield (E_{PVT}, kWh) of the PV-T collectors:

$$E_{PVT} = p_{PVT} \cdot \Delta t \tag{6}$$

- HP thermal energy generated (Q_{HP}, kWh):

$$Q_{HP} = q_{HP} \cdot \Delta t \tag{7}$$

- HP electricity consumption (E_{HP}, kWh):

$$E_{HP} = p_{HP} \cdot \Delta t \tag{8}$$

- Electrical solar contribution factor to the rev-HP (SCF_{eHP}):

$$SCF_{eHP} = \frac{E_{PVT}}{E_{HP}} \tag{9}$$

- Thermal solar contribution factor (SCF_{th}):

$$SCF_{th} = \frac{Q_{PVT}}{Q_{heating} + Q_{DHW}} \tag{10}$$

3. Results and discussion

The validation of the solar system model is performed in three main steps. First, the model of the PV-T collectors is validated against the experimental data of the pilot plant (Section 3.2). Then, the air-to-water heat pump is validated using a simplified transient model along with the monitoring data (Section 3.3). Once the two main components are validated, the overall solar system model is run using the real weather data and the real building energy demand as inputs, and the simulation results are compared with the experimental data.

3.1. Input parameters of the solar hybrid pilot plant

To analyse the performance of the solar hybrid pilot plant and validate the transient model, several performance parameters and demand set-points are varied. Table 5 summarises the values set for the parameters during the operating weeks used to validate the transient model. The set-point temperatures for space heating/cooling refer to the temperature of the water leaving the HP and entering the fan-coils to provide heating/cooling.

Fig. 4 shows as an example the weather conditions (solar irradiance, ambient temperature and wind speed) from February 8th until March 8th, 2021. These data are inputs in the transient model, with the experimental data averaged every 5-min to match the simulation time step.

Table 5
Summary of input parameters.

Week		8–14 Feb	15–21 Feb	22–28 Feb	1–7 Mar
Set-point DHW	[°C]	50	50	50	50
Set-point space heating	[°C]	40	40	45	45
PV-T collector flow-rate	[l/h·m^2]	50	30	30	50
Week		**10–16 Mar**	**17–23 Mar**	**4–10 May**	**11–17 May**
Set-point DHW	[°C]	–	–	50	50
Set-point space heating	[°C]	40	40	–	–
PV-T collector flow-rate	[l/h·m^2]	50	30	50	50
Week		**15–21 Jul**	**22–29 Jul**	**2–8 Aug**	**19–25 Aug**
Set-point space cooling	[°C]	7	7	7	7
PV-T collector flow-rate	[l/h·m^2]	30–40	30–40	30–40	30–40

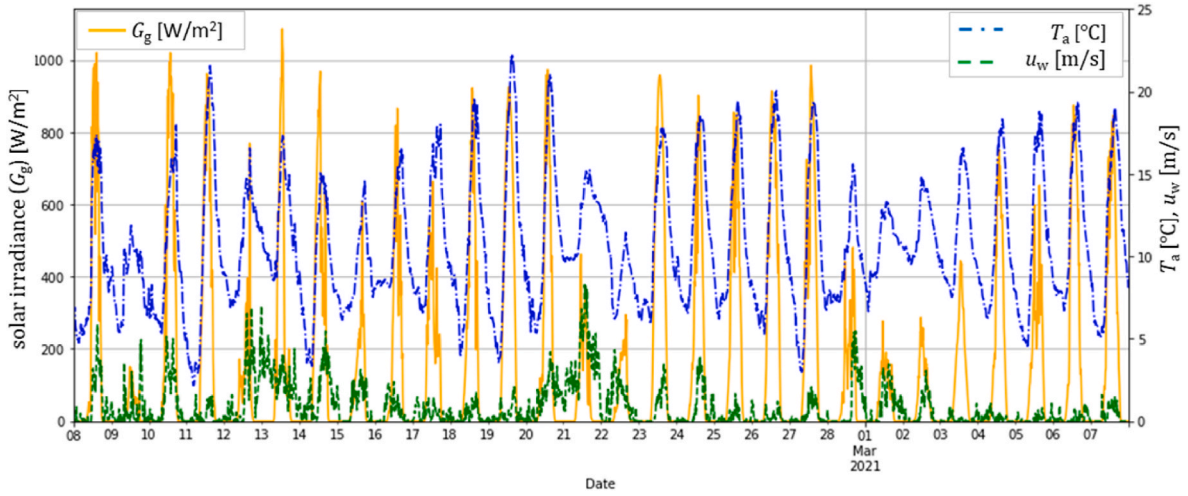

Fig. 4. Sample of weather conditions during the experimental tests.

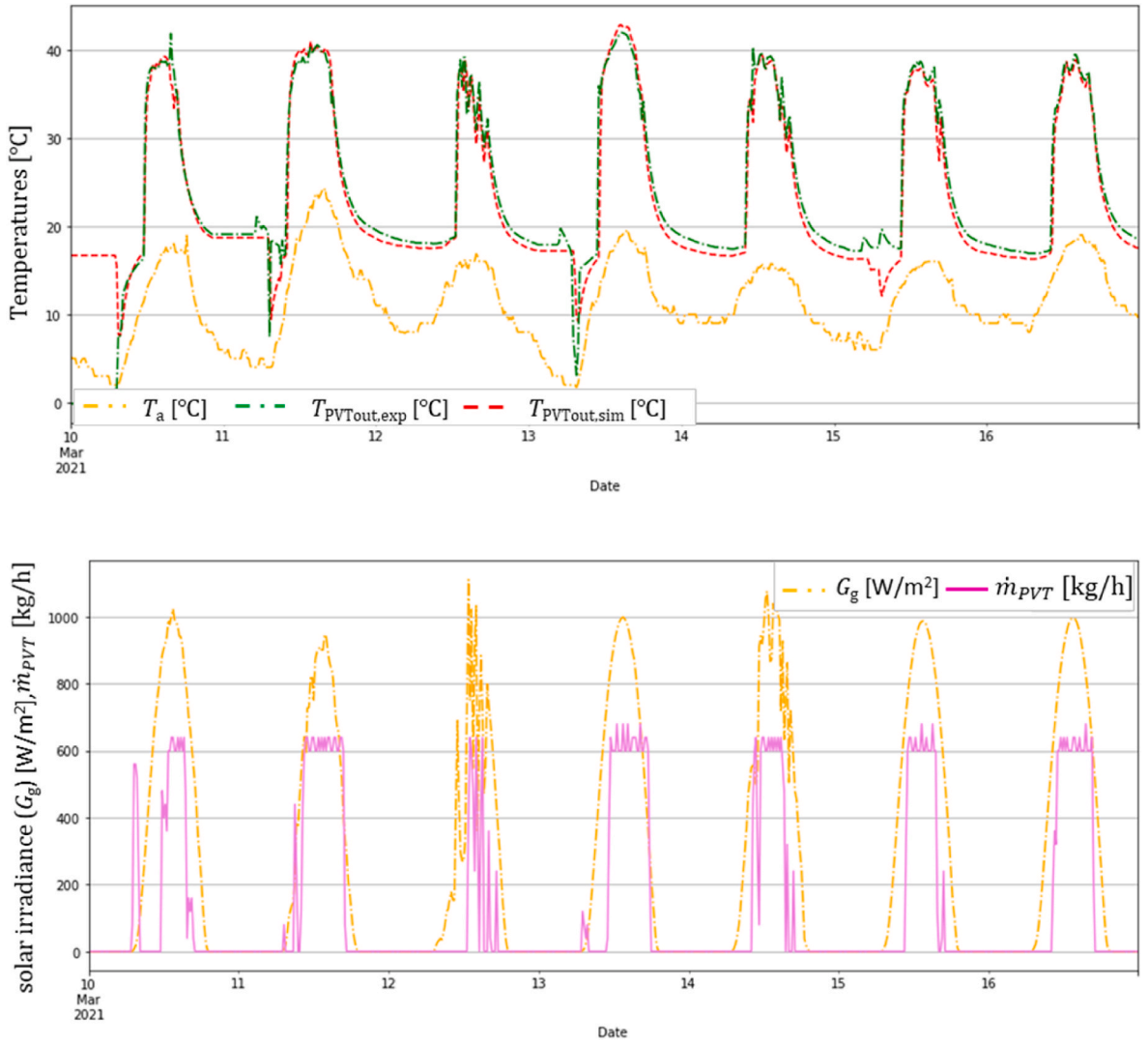

Fig. 5. (Top) outlet temperature of the PV-T collectors (T_{PVTout}) according to the transient model (sim), and experimental data (exp); (bottom) solar irradiance (G_g [W/m^2]) and PV-T collector flow-rate ($\dot{m}_{PVT}$ [kg/h]), during the week 10th-16th March 2021.

3.2. PV-T collectors

First, the performance of the PV-T collectors is validated against the experimental data from the pilot plant. Here, the inlet water temperature and the collector flow rate are inputs to the transient model, as well as the weather conditions.

As shown in Fig. 5, the simulation results are in good agreement with the experimental data. The outlet water temperature reaches 38–42 °C during the high solar irradiance hours. The weekly-averaged error of the outlet water temperature during the week 10th-16th March 2021 shown in Fig. 5 is 2%, which means that the model slightly overestimates the PV-T outlet water temperature. The main differences are observed when solar irradiance is very low, particularly at the beginning of the day (see 11th, 13th and 15th of March). This might be due to the thermal response of the PV-T collectors, as, in reality, PV-T collectors have stagnant cold water at the beginning of the day. Instead, the simulation only considers the inlet water temperature, not considering the cold water mass inside the collector. As a consequence, water gets warmer sooner in the model when circulating at the beginning of the day.

Fig. 6 also shows that the electricity generation estimated in the transient model matches the real electricity generation measured in the pilot plant. For instance, the weekly-averaged error during the week 10th-16th March 2021 shown in Fig. 6 is -1%, which means that the model slightly underestimates the PV-T electricity output. In this case, larger discrepancies occur when solar irradiance is high. Here it should be noted that the pilot plant does not monitor the PV-T cell temperature, so the estimated cell temperature in the transient model cannot be compared with experimental data.

Looking at the weekly results, it is observed that the average outlet temperature of the PV-T collectors (T_{PVTout}) obtained in the transient model is in general slightly overestimated, with a maximum error of 6% and an average error for all weeks analysed of 3% (Fig. 7).

The electrical (η_e) and thermal (η_{th}) efficiencies of the PV-T collectors during the analysed weeks (see Table 5) are shown in Fig. 8. There are larger differences in thermal energy efficiency. The average thermal efficiency over the analysed weeks according to the pilot plant model is 12.5%, while the average experimental thermal efficiency is 11.2%. That is, the transient model predicts the PV-T thermal efficiency with an average error of 12% over the analysed weeks. In general, the thermal efficiency is also overestimated in the model, in agreement with the estimated outlet temperature of the PV-T collectors. The maximum thermal efficiency occurs the week of July 22–29th, 19.2% according to the pilot plant model, and 16.9% according to experimental data (14% error). This might be attributed to an underestimation of the thermal losses under certain weather conditions. As shown in Fig. 3, at high wind speeds and low solar irradiance conditions, the PV-T collector model overestimates the thermal efficiency.

The estimated electrical efficiencies accurately represent the actual efficiencies. The average electrical efficiency over the analysed weeks according to the pilot plant model is 16.1%, while the average experimental electrical efficiency is 15.8% (thus an average error of 2.5%). The maximum electrical efficiency occurs the week of March 1–7th, 16.7% according to the pilot plant model, and 16.3% according to experimental data (1% error). Therefore it can be concluded that PV-T collector model reproduces accurately the actual performance of the PV-T collectors.

3.3. Air-to-water reversible heat pump

Similarly, the performance of the rev-HP is validated against experimental data from the pilot plant. Here, the rev-HP inlet temperature (T_{HPin}) and rev-HP flow rate are inputs to the model, as well as the weather conditions (e.g. ambient temperature), to compare the results.

The rev-HP is validated first during two weeks with the pilot plant operating in heating mode to satisfy only heating demand (10th-23rd March), then during the two weeks with only DHW demand (4th-17th May), and finally during two weeks with only cooling demand (15th-29th July).

A simplified transient model of the pilot plant is developed for this validation, including only the rev-HP and the corresponding storage tank, that is, the hot-water tank for the validation of the rev-HP to provide DHW, and the inertia tank for the validation of the rev-HP to provide space heating or cooling (see Fig. 9).

3.3.1. Heating mode

As shown in Table 5, during the weeks 10th-23rd March the pilot plant operated in heating mode to satisfy the space heating demand at 40 °C. The first week the PV-T collector flow rate was set at 50 l/h·m^2 and the second one at 30 l/h·m^2.

The results show that, in general, the estimated thermal power generated by the rev-HP for heating (green line in Fig. 10) is in agreement with the experimental data (red line). Larger differences occur at the beginning of the day at the HP start-up. Some days, the first thermal power peak is underestimated (e.g. on the 10th, 13th or 23rd of March), on other days it is overestimated (e.g. on the 17th, 18th or 22nd of March), and on others, it is accurately predicted (e.g. on the 12th or 15th of

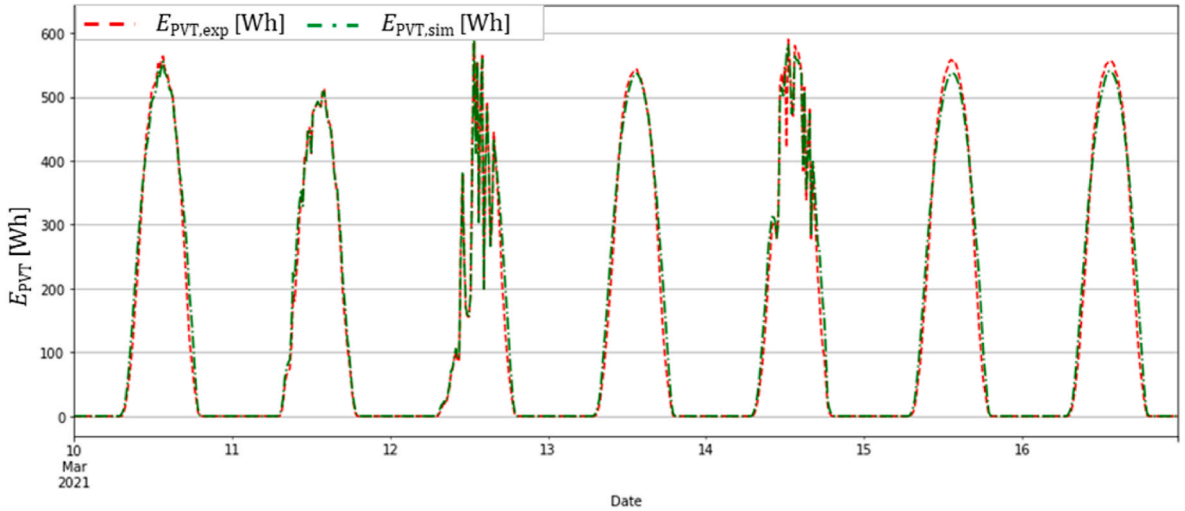

Fig. 6. Electricity generation of the PV-T collectors estimated by the transient model (sim) and from the experimental data (exp) during the week 10th-16th March 2021.

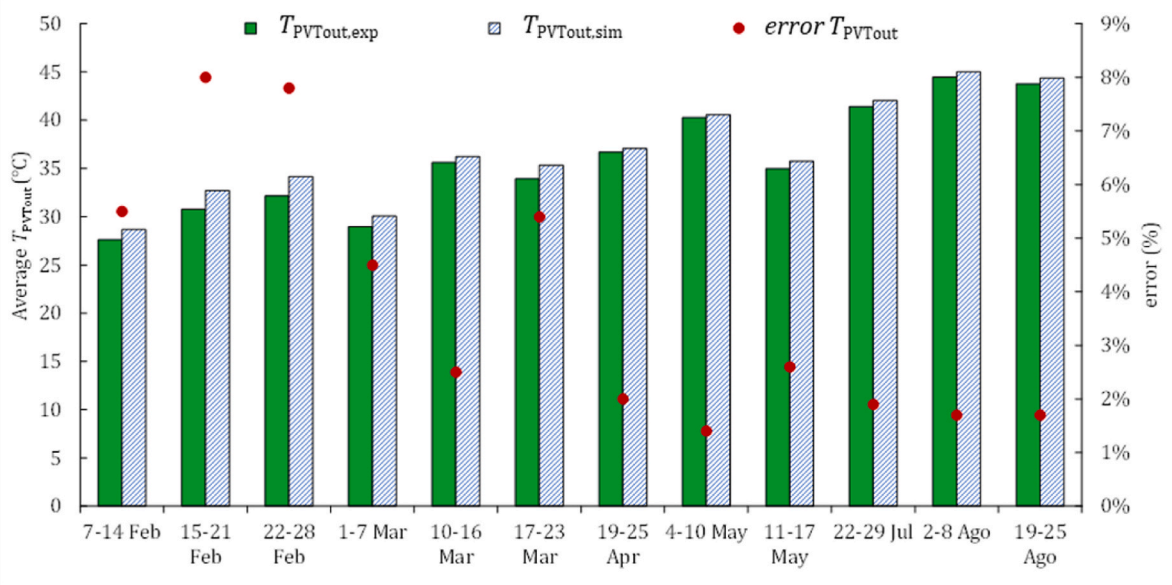

Fig. 7. Weekly average PV-T outlet temperature (T_{PVTout}) estimated by the transient model (sim), and from the experimental data (exp) in the analysed weeks.

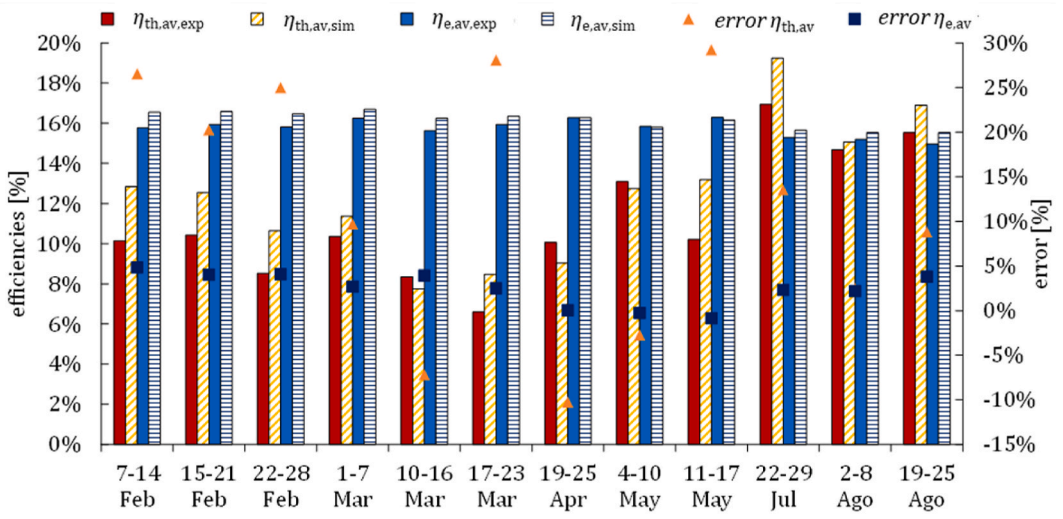

Fig. 8. Electrical (η_e) and thermal (η_{th}) efficiencies of the PV-T collectors estimated by the transient model (sim), and from experimental data (exp), and corresponding errors in the analysed weeks.

March). Similar results are obtained by comparing the electrical power consumed by the rev-HP (see Fig. 11).

It is also observed that the performance on some days is predicted more accurately than on others. Here it should be noted that it is not possible to accurately model the performance of the rev-HP at partial load for two main reasons. First, the HP manufacturer does not provide data on thermal generation, consumption and/or COP of the rev-HP at partial load, while the HP works with a variable speed compressor. Also, the transient model of the rev-HP does not allow to include the performance data at partial load. As a consequence, the rev-HP model works at full power until the demand set-point is reached.

Fig. 12 shows that, in general, the DHW supply temperature (T_{DHW}) according to the model (green line) fits the experimental data (red line). The main differences occur also at the beginning of the day at the HP start-up. It is also observed that the estimated temperature at the bottom of the hot-water storage tank (T_{tBot}, blue line) follows the same trend as the experimental temperature (yellow), particularly when there is hot-water contribution from the PV-T collector circuit (violet line). During the evening the measured temperature drops further than the modelled one, which might be due to an underestimation of the tank thermal losses.

The weekly analysis shows that the thermal energy generated by the rev-HP (Q_{HP}) according to the model has an error between -36% and -6%, with an average error of -24%. Meanwhile, the average error of the electricity consumption of the rev-HP (E_{HP}) is -13%, ranging between -31% and 9%, depending on the analysed week. That is, in general, the model underestimates the thermal energy generation and electricity consumption of the rev-HP (see Fig. 13). This is attributed to two main reasons. First, the model assumes that the rev-HP operates at full load and constant compressor speed, considering the thermal capacity and power facilitated by the manufacturer at the different temperature conditions at nominal compressor speed.

Furthermore, during the winter weeks (February and March), the pilot plant was operating an anti-freezing mode at night, which activated the PV-T collector circuit when the ambient temperature was below 6 °C. Consequently, the cold water exiting the PV-T collectors

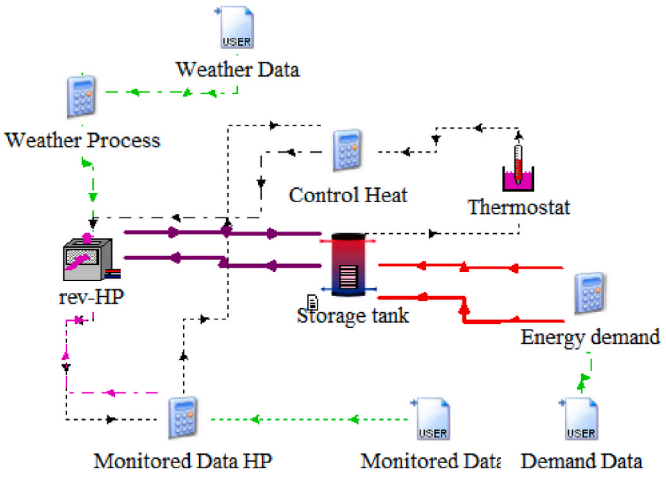

Fig. 9. Transient model developed for the validation of the rev-HP.

cooled down the inertia tank at night, and the rev-HP had to heat further the tank at the beginning of the next day. However, this anti-freezing mode has not been considered in the transient model. This also explains the larger peak of the thermal power generated by the rev-HP in the experimental data (see for instance the 10th and 13th of March in Fig. 10).

Fig. 13 shows that the COP of the rev-HP according to the model is closer to the experimental one. The COP in heating mode is 3.7–3.8 according to the simulation model, while the experimental data shows COPs of 4.3–4.4 (weekly-averaged error of -14%). Meanwhile, the COP in DHW mode is 3.7–3.8 (simulation model) vs. 4.1–4.3 (experimental data), thus a weekly-averaged error of -7% or -15% depending on the week. Therefore, the model also underestimates the COP. Considering that the main input to the rev-HP model to reproduce its real performance is its thermal capacity and power (thus the COP) at different operating temperatures, it is believed the rev-HP model reproduces adequately the actual performance of the rev-HP because the COP is estimated with an average error of -13% over the weeks when it operates

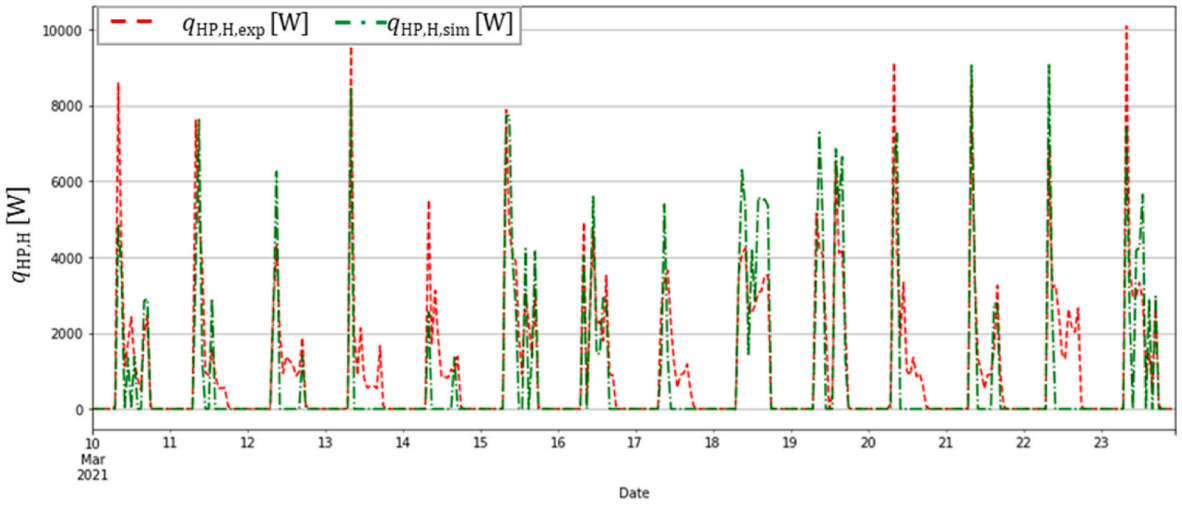

Fig. 10. Thermal power generated by the rev-HP for heating ($q_{HP,H}$) according to the model (sim) and experimental data (exp) in heating mode from the 10th to the 23rd of March 2021.

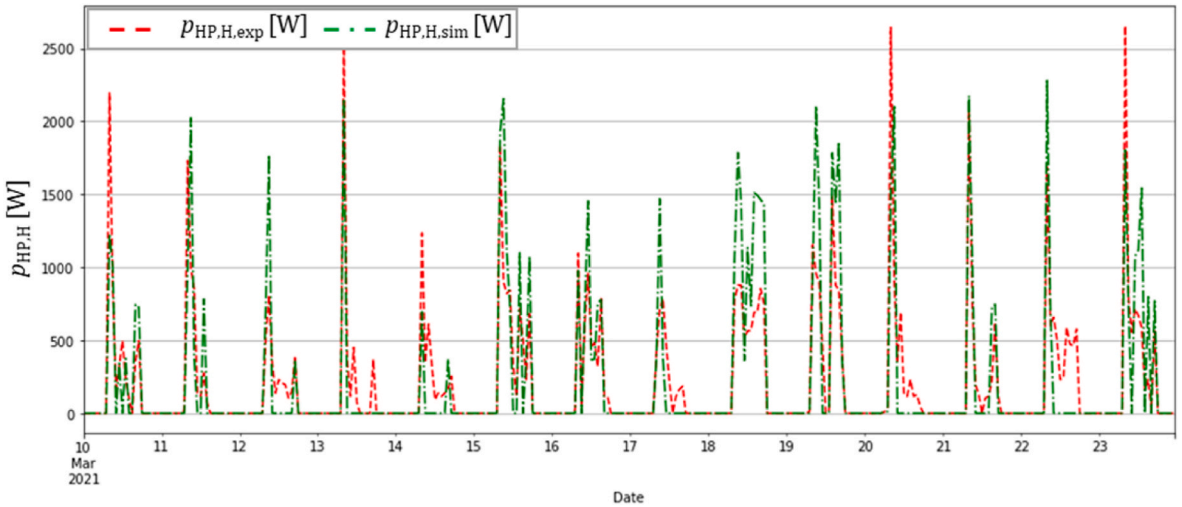

Fig. 11. Electrical power consumed by the rev-HP for heating ($p_{HP,H}$) according to the model (sim) and experimental data (exp) in heating mode from the 10th to the 23rd of March 2021.

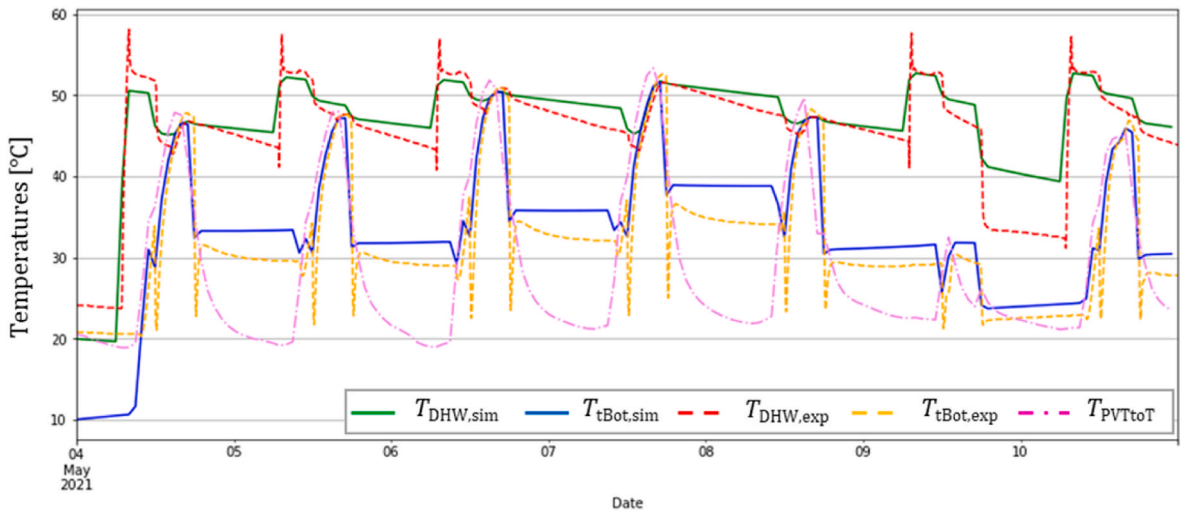

Fig. 12. DHW temperature (T_{DHW}) according to the model (sim) and experimental data (exp), temperature of the PVT circuit entering the hot-water tank (T_{PVTtoT}), and temperature at the bottom of the hot-water tank (T_{tBot}) according to the model (sim) and experimental data (exp) from the 4th to the 10th of May 2021.

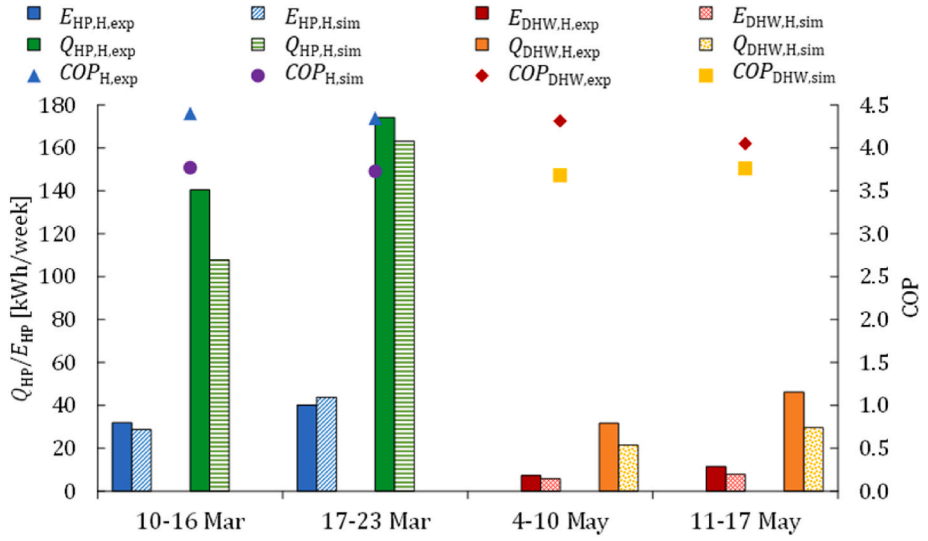

Fig. 13. Electricity consumption (E_{HP}) and thermal energy generated (Q_{HP}) by the rev-HP according to the model (sim) and experimental data (exp) in heating mode for heating provision (H) or DHW provision (DHW).

heating water.

3.3.2. Cooling mode

In summer, the pilot plant operated in cooling mode to satisfy the space cooling demand; with water leaving the HP and entering the fan-coils at 7 °C (see Table 5). The PV-T collector flow rate was set at 30–40 l/h·m^2.

Fig. 14 shows that the estimated cooling power of the rev-HP (green line) is in agreement with the experimental data (red line). Similar to the heating mode, larger differences occur at the beginning of the day at the HP start-up. In this case, most of the days the first thermal power peak is underestimated, which is compensated later in the day with an overestimation of the cooling thermal power. On a weekly basis, the cooling thermal power (Q_{HP}) is overestimated by 10–12% (see Fig. 17).

Similar results are obtained comparing the electrical power consumed by the rev-HP (see Fig. 15), but in this case, the weekly-averaged error is lower, from -2.2% to -2.6% (see Fig. 17). In cooling mode, the PV-T thermal output is fed to the hot-water tank, while the rev-HP cools down the inertia tank to provide cooling, so both circuits are independent. This might explain the lower error in the estimated rev-HP performance in cooling mode.

The estimated COP also follows the experimental data during these weeks, as shown in Fig. 16. The COP in cooling mode is 3.4–3.5 according to the simulation model, while the experimental data shows COPs of 3.0–3.1 (weekly-averaged error of 13–14%). Thus, in this case, the model overestimates the COP.

3.4. Summary of the energy performance results

Once the main components are individually validated, the performance of the overall pilot plant is analysed and validated, for which the full transient model is run with a 5-min time step with the input parameters stated in Table 2. In this section, the overall results during the first four weeks of operation are shown and discussed. These weeks are selected because the rev-HP provides both DHW and heating demands, so both storage tanks are in operation as well as the control system to direct the PV-T thermal output to either of the tanks.

Fig. 18 shows that the electrical generation of the PV-T collectors is slightly overestimated by the transient model, by 3% on average. The PV-T electrical output varies between 46.5 kWh/week and 63 kWh/

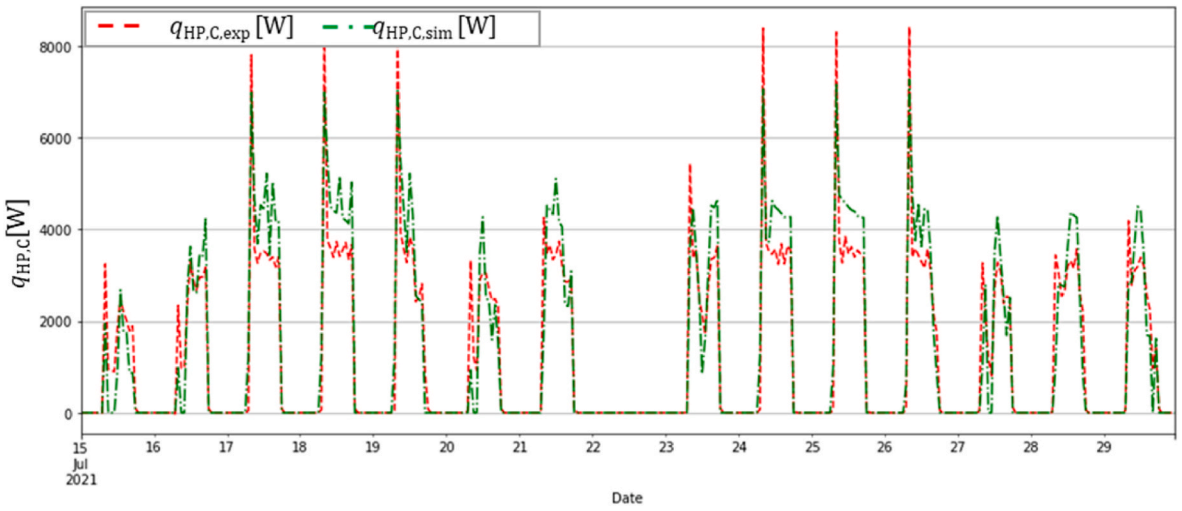

Fig. 14. Thermal power generated by the rev-HP for cooling ($q_{HP,C}$) according to the model (sim) and experimental data (exp) in cooling mode from the 15th to the 29th of July 2021.

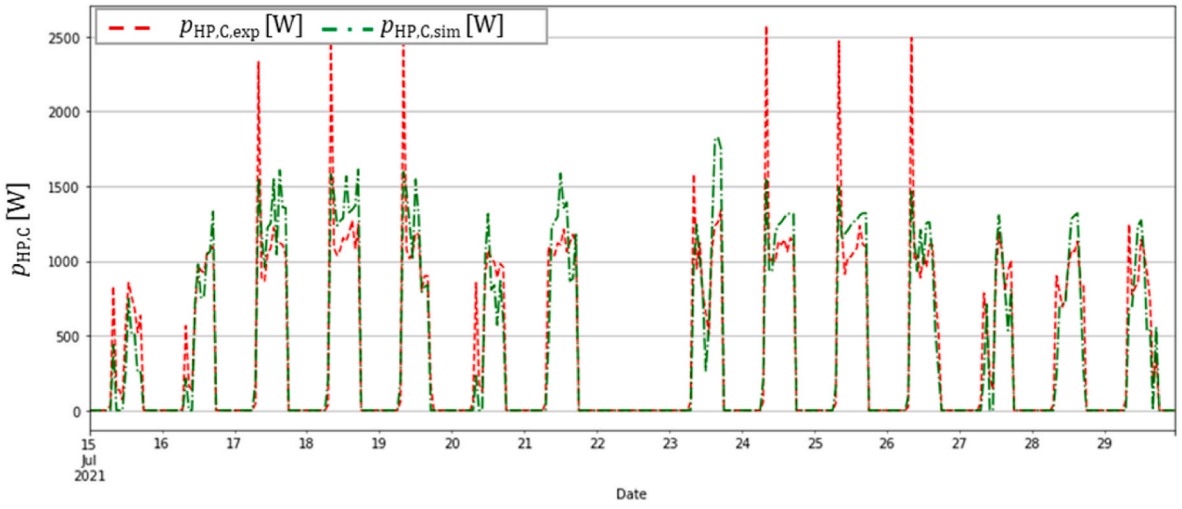

Fig. 15. Electrical power consumed by the rev-HP for cooling ($p_{HP,C}$) according to the model (sim) and experimental data (exp) in cooling mode from the 23rd to the 29th July 2021.

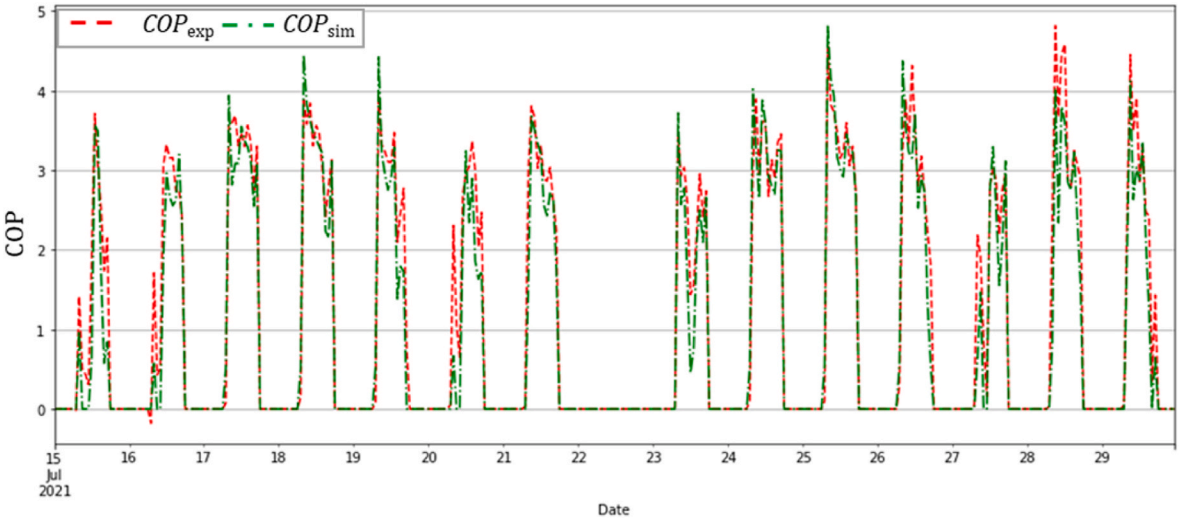

Fig. 16. COP of the rev-HP according to the model (sim) and experimental data (exp) in cooling mode from the 23rd to the 29th of July 2021.

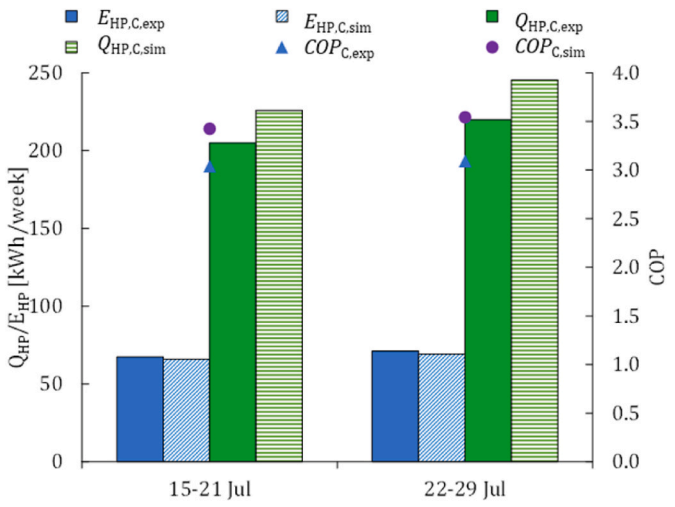

Fig. 17. Electricity consumption (E_{HP}) and thermal energy (Q_{HP}) of the rev-HP according to the model (sim) and experimental data (exp) in cooling mode in the analysed weeks.

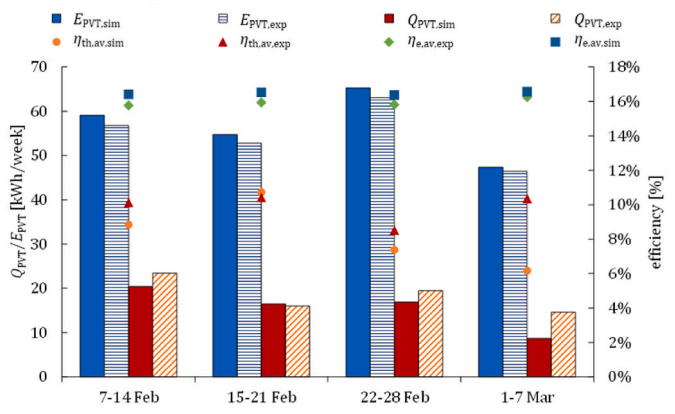

Fig. 18. Electricity (E_{PVT}) and thermal energy (Q_{PVT}) generation of the PV-T collector field, and average (av) electrical (η_e) and thermal (η_{th}) efficiencies, according to the model (sim) and experimental data (exp).

week experimentally and between 47.4 kWh/week and 65.2 kWh/week according to the simulation. The thermal energy generation ranges from 14.6 kWh/week to 23.4 kWh/week experimentally and from 8.7 kWh/week to 20.4 kWh/week according to the simulation, being in general underestimated, by -16% on average. The lower thermal efficiency estimated by the model is attributed to the higher temperature of the water circulating through the PV-T collectors in the transient model. As mentioned in the previous section, during the winter months the pilot plant had active an anti-freezing mode for the PV-T circuit, which cooled down the storage tank at night. Consequently, the temperature of the water entering the PV-T collector at the beginning of the next day is lower in the pilot plant than in the model, leading to a larger experimental thermal efficiency (see triangles in Fig. 18).

Table 6 summarises the main energy performance results and key performance indicators of the pilot plant according to the simulation results (sim) and experimental data (exp).

The space heating demand estimated by the model has an error between -19% and 19%, with values within 91.2–183 kWh/week (experimentally) and 84.3–200.2 kWh (simulation). The average error over the four weeks is 1%, so the heating demand is balanced out during the weeks. The DHW demand estimated by the model has an error between 11% and 15%, and an average error of 12%, being in general overestimated by the model. The differences are attributed to the supply

Table 6
Summary of the energy performance results and key performance indications according to the simulation (sim) and experimental (exp) data.

Week	Unit	8–14 Feb	15–21 Feb	22–28 Feb	1–7 Mar
Average G_g	[W/m^2]	350.6	311.2	366.2	257.1
Average T_a	[°C]	12.5	13.2	13.0	13.3
Q_{PVT} (exp)	[kWh]	23.4	16.0	19.4	14.6
Q_{PVT} (sim)	[kWh]	20.4	16.4	16.9	8.7
E_{PVT} (exp)	[kWh]	56.8	52.8	63.0	46.5
E_{PVT} (sim)	[kWh]	59.1	54.7	65.2	47.4
error Q_{PVT}	[%]	-12.8%	2.9%	-13.3%	-40.4%
error E_{PVT}	[%]	4.1%	3.7%	3.5%	2.0%
η_{th} (exp)	[%]	10.1%	10.4%	8.5%	10.4%
η_{th} (sim)	[%]	8.8%	10.7%	7.4%	6.2%
η_e (exp)	[%]	15.8%	15.9%	15.8%	16.3%
η_e (sim)	[%]	16.4%	16.5%	16.4%	16.6%
$Q_{heating}$ (exp)	[kWh]	112.9	155.4	183.0	91.2
$Q_{heating}$ (sim)	[kWh]	134.4	126.6	200.2	84.3
error $Q_{heating}$	[%]	19%	-19%	9%	-8%
Q_{DHW} (exp)	[kWh]	13.0	13.9	21.4	24.0
Q_{DHW} (sim)	[kWh]	14.6	15.5	23.7	27.7
error Q_{DHW}	[%]	12%	11%	11%	15%
Q_{HP} (exp)	[kWh]	197.9	217.5	269.0	188.7
Q_{HP} (sim)	[kWh]	155.8	132.6	218.2	115.4
error Q_{HP}	[%]	-21%	-39%	-19%	-39%
E_{HP} (exp)	[kWh]	44.4	49.3	60.1	41.7
E_{HP} (sim)	[kWh]	38.2	32.2	54.5	29.8
error E_{HP}	[%]	-14%	-35%	-9%	-29%
COP_{HP} (exp)	[−]	4.45	4.41	4.48	4.52
COP_{HP} (sim)	[−]	4.08	4.11	4.00	3.87
error COP_{HP}	[%]	-8%	-7%	-11%	-14%
SCF_{eHP} (exp)	[−]	1.28	1.07	1.05	1.11
SCF_{eHP} (sim)	[−]	1.55	1.70	1.20	1.59
SCF_{th} (exp)	[−]	0.19	0.09	0.10	0.13
SCF_{th} (sim)	[−]	0.14	0.12	0.08	0.08

temperature, which varies a few degrees above and below the set-point temperature both in the simulation and in the experimental data, as the rev-HP goes on and off at the different time steps.

There are larger differences regarding the thermal energy generated and electricity consumed by the rev-HP. Specifically, the transient model underestimates the thermal generation of the rev-HP by -30%, on average, and the HP electricity consumption by -22%, on average. This is attributed to the reasons discussed above. The model assumes that the rev-HP operates at full load and constant (nominal) compressor speed. Meanwhile, the actual rev-HP has quick dynamics, in which the compressor operates at variable speed, according to the thermal load; the lower the thermal load, the lower the compressor speed and the corresponding power consumption. However, the transient model (Type 941) does not allow varying the compressor speed, so the accuracy of the HP model decreases when the rev-HP is not working at nominal speed.

Another reason is that the model does not consider the anti-freezing mode of the PV-T circuit in winter. This anti-freezing mode cools down the inertia tank of the pilot plant at night, so at the beginning of the day, more heat is required to satisfy the space heating demand at its set-point (e.g. larger experimental Q_{HP}), and thus more electricity is consumed by the rev-HP (e.g. larger experimental E_{HP}). Still, Table 6 shows that the rev-HP COP estimated in the transient model is similar to the one obtained in the pilot plant, with estimated values of 3.87–4.11 and experimental values of 4.41–4.52. The average error over the four weeks is -10%, that is, the COP is underestimated on average.

The electrical solar contribution factor to the rev-HP (SCF_{eHP}) is larger than 1 in any of the analysed weeks, with an average value of 1.13 (experimentally) and 1.51 (simulation) over the four weeks. This means that the PV-T electricity generation is larger than the rev-HP electricity consumption, and therefore the electricity surplus can be used to satisfy the rest of the electricity consumption of the building. The SCF_{eHP} is estimated with an average error over the four weeks of 34%, so the model overestimates the electrical solar contribution factor.

On the thermal side, only a small amount of the thermal energy

demand can be satisfied by the PV-T thermal output in the winter weeks shown in this work; 13% and 10%, on average, according to the experimental and simulation results, respectively. The thermal solar contribution factor is, in general, underestimated by the model, with an average error over the four weeks of -16%.

The results for the summer months show that, with the electrical and thermal generation of the PV-T collectors (see Fig. 7), it is possible to cover all the electricity consumed by the rev-HP to satisfy the space cooling demand ($SCF_{eHP} > 1$) as well as all the DHW demand ($SCF_{th} > 1$). Detailed results of the experimental performance of the pilot plant can be found in previous work by the authors [87].

4. Further discussion

The validation results of the main components of the pilot plant are very promising. The maximum thermal efficiency obtained (19.2%) is in line with previous studies that analysed an uncovered PV-T collector with a similar absorber design [96]. Electrical efficiencies (~16%) are also in agreement with previous theoretical [97] and experimental works [98]. The energy performance of the PV-T collectors obtained with the transient model fits the experimental data, with an average error of -16% and 3% for the thermal and electrical generation respectively. The lower thermal efficiency estimated by the full pilot plant model is mainly attributed to the higher temperature of the water circulating through the PV-T collectors in the winter months analysed, due to the activation of the anti-freezing mode in the actual pilot plant, which is not considered in the model. The PV-T collector model can thus be used to estimate the performance of this type of PV-T collector in different weather conditions or integrated with other components (e.g. other type of HP or storage tanks). To model other type of PV-T collector (e.g. glazed PV-T collector), the model should be modified accordingly to fit the performance of the specific collector.

The COP values of the analysed rev-HP (3.7–3.8 in heating mode) are in agreement with previous research [70]. The estimated COP obtained in cooling mode (3.4–3.5) is also in line with previous works [55]. Here, it should be highlighted that the COP of an HP strongly depends on the type of HP and on the specific location of the system, as shown in the literature review of Section 1. Therefore, the HP model should be modified to simulate other types of HPs (such as water-to-water HPs) to fit the real performance.

The results show that the PV-T electricity generation can cover all the rev-HP energy consumption throughout the year, with some electricity surplus that can be used to satisfy the rest of the electricity consumption of the building. In the winter months, the PV-T thermal output can only cover a small percentage of the building thermal energy demand. This is attributed to the low temperatures and low solar irradiance levels of the winter weeks. Instead, in the summer months, the PV-T thermal generation can cover all the DHW demand.

5. Conclusion

This work presents the main validation results of the transient model of a solar hybrid system that consists of PV-T collectors integrated with an air-to-water rev-HP. The pilot plant, composed of eight uncovered PV-T collectors (2.6 kW_e, 13.6 m^2), two water storage tanks (of 350 l for DHW and 263 l for space heating/cooling) and a commercial rev-HP, is currently in operation in ENDEF facilities located in Zaragoza (Spain).

The main finding of this work concerns the rev-HP performance, which shows the largest differences with experimental data. The accuracy of the estimated rev-HP performance depends on the operation mode. This is attributed to two main reasons. First, the model assumes that the rev-HP operates at full load and constant (nominal) compressor speed. Meanwhile, in reality, the rev-HP compressor speed and thermal capacities vary depending on the thermal energy required, controlled by a PID controller internal to the HP. However, the HP manufacturer does not provide data on the rev-HP performance at partial load and variable compressor speed. Therefore, specific performance tests would be required in a controlled chamber to characterise the HP performance at different loads. Then, this performance data at partial loads should be modelled in a new component type of the HP model that allows this integration or in an ad-hoc HP model.

Another reason for the deviation between the experimental and simulated HP performance is the anti-freezing mode, which was active in the pilot plant in the winter months. This operation mode led to active cooling of the inertia tank at night, and thus more heat was required at the beginning of the day to satisfy the space heating demand at its set-point. This would explain why the simulation results in cooling mode fit more accurately the experimental data, as in summer months the PV-T thermal output is fed to the hot-water tank, while the rev-HP cools down the inertia tank to provide cooling, so both circuits are independent.

The results show that the rev-HP COP estimated in the transient model is similar to the one obtained in the pilot plant, with an average error of -10%. Therefore, considering that the main input to the rev-HP model to reproduce its real performance is its thermal capacity and power (thus the COP) at different operating temperatures, it is concluded the rev-HP model reproduces adequately the actual performance of the rev-HP.

The energy performance of the PV-T collectors obtained with the transient model is also in agreement with the experimental data, with an average error of -16% and 3% for the thermal and electrical generation respectively. The validated model can thus be used to optimise the system performance, as well as to size the main components and analyse the system performance under different climates and satisfy diverse energy demands, minimising the need for lengthy and expensive experimental works. The modelling results can then be used to perform economic and environmental analyses and assess the potential of the proposed solar system at a wider scale.

The results show that thanks to the simultaneous electricity and thermal generation of the PV-T collectors, together with the high performance of the rev-HP, the pilot plant is overall self-sufficient to satisfy the building energy demand.

Proposed further work includes an in-depth analysis of the rev-HP performance to characterise experimentally its performance at different compressor speeds and different loads. Then, include this performance data in a new component type of the HP model that allows this integration or develop an ad-hoc HP model, to improve the simulation of the HP dynamic behaviour operating at variable speed. Furthermore, new experiments are planned in the pilot plant that include the analysis of its performance in winter without the influence of the anti-freezing mode, for instance using a separate small tank to dump the cold water at night.

Credit author statement

María Herrando: Conceptualization, Methodology, Software, Validation, Formal analysis, Investigation, Data curation, Visualization, Writing – original draft, Writing – review & editing. **Adriana Coca-Ortegón:** Methodology, Formal analysis, Data curation, Writing – review & editing. **Isabel Guedea:** Resources, Writing – review & editing, Project administration, Funding acquisition. **Norberto Fueyo:** Writing – review & editing, Visualization, Supervision, Project administration, Funding acquisition.

Declaration of competing interest

The authors declare that they have no known competing financial interests or personal relationships that could have appeared to influence the work reported in this paper.

Data availability

Data will be made available on request.

Acknowledgements

This work was undertaken in the framework of the 3GSol project, funded under the Retos-Colaboración 2017 Programme, National R&D and Innovation Plan, by the Spanish Government, Ministry of Science, Innovation and Universities and cofunded by the EU (through the European Regional Development Fund (ERDF)) [grant number RTC-2017-6026-3]. We also acknowledge funding to the group of Computational Fluid Mechanics from the Regional Government of Aragón [Group T32_20 R].

References

[1] European Commission. EU energy in Figures. 2021. https://doi.org/10.2833/87498.
[2] Herrando M, Ramos A. Photovoltaic-thermal (PV-T) systems for combined cooling, heating and power in buildings: a review. Energies 2022;15. https://doi.org/10.3390/en15093021.
[3] European Commission. An EU strategy on heating and cooling. Communication from the Commission to the European Parliament. the Council, the European Economic and Social Committee and the Committee of the Regions; 2016.
[4] Østergaard PA, Duic N, Noorollahi Y, Kalogirou S. Renewable energy for sustainable development. Renew Energy 2022;199:1145–52. https://doi.org/10.1016/J.RENENE.2022.09.065.
[5] Østergaard PA, Duic N, Noorollahi Y, Kalogirou SA. Recent advances in renewable energy technology for the energy transition. Renew Energy 2021;179:877–84. https://doi.org/10.1016/J.RENENE.2021.07.111.
[6] Herrando M, Simón R, Guedea I, Fueyo N. Solar combined cooling, heating and power systems based on hybrid PVT, PV or solar-thermal collectors for building applications. 14th Conf. Sustain. Dev. Energy, Water Environ. Syst. SDEWES2019.0114 2019:1–15. https://doi.org/10.1016/j.renene.2019.05.004. Dubrovnik.
[7] Ekins-Daukes NJ. Solar energy for heat and electricity: the potential for mitigating climate change. Grantham Inst Clim Chang 2009;1:1–12.
[8] Yang C. Reconsidering solar grid parity. Energy Pol 2010;38:3270–3. https://doi.org/10.1016/j.enpol.2010.03.013.
[9] Ge TS, Wang RZ, Xu ZY, Pan QW, Du S, Chen XM, et al. Solar heating and cooling: present and future development. Renew Energy 2018;126:1126–40. https://doi.org/10.1016/J.RENENE.2017.06.081.
[10] Leonzio G. Solar systems integrated with absorption heat pumps and thermal energy storages: state of art. Renew Sustain Energy Rev 2017;70:492–505. https://doi.org/10.1016/J.RSER.2016.11.117.
[11] Montagnino FM. Solar cooling technologies. Design, application and performance of existing projects. Sol Energy 2017;154:144–57. https://doi.org/10.1016/J.SOLENER.2017.01.033.
[12] Drosou VN, Tsekouras PD, Oikonomou TI, Kosmopoulos PI, Karytsas CS. The HIGH-COMBI project: high solar fraction heating and cooling systems with combination of innovative components and methods. Renew Sustain Energy Rev 2014;29:463–72. https://doi.org/10.1016/j.rser.2013.08.019.
[13] Li YW, Wang RZ, Wu JY, Xu YX. Experimental performance analysis on a direct-expansion solar-assisted heat pump water heater. Appl Therm Eng 2007;27:2858–68. https://doi.org/10.1016/j.applthermaleng.2006.08.007.
[14] Thygesen R, Karlsson B. Simulation and analysis of a solar assisted heat pump system with two different storage types for high levels of PV electricity self-consumption. Sol Energy 2014;103:19–27. https://doi.org/10.1016/j.solener.2014.02.013.
[15] Fong KF, Lee CK, Chow TT. Comparative study of solar cooling systems with building-integrated solar collectors for use in sub-tropical regions like Hong Kong. Appl Energy 2012;90:189–95. https://doi.org/10.1016/J.APENERGY.2011.06.013.
[16] Protopapadaki C, Saelens D. Heat pump and PV impact on residential low-voltage distribution grids as a function of building and district properties. Appl Energy 2017;192:268–81. https://doi.org/10.1016/j.apenergy.2016.11.103.
[17] Mellor A, Alonso Alvarez D, Guarracino I, Ramos A, Riverola Lacasta A, Ferre Llin L, et al. Roadmap for the next-generation of hybrid photovoltaic-thermal solar energy collectors. Sol Energy 2018;174:386–98. https://doi.org/10.1016/j.solener.2018.09.004.
[18] Das D, Kalita P, Roy O. Flat plate hybrid photovoltaic- thermal (PV/T) system: a review on design and development. Renew Sustain Energy Rev 2018;84:111–30. https://doi.org/10.1016/j.rser.2018.01.002.
[19] Herrando M, Ramos A, Zabalza I, Markides CN. A comprehensive assessment of alternative absorber-exchanger designs for hybrid PVT-water collectors. Appl Energy 2019;235:1583–602. https://doi.org/10.1016/J.APENERGY.2018.11.024.
[20] Joshi SS, Dhoble AS. Photovoltaic -Thermal systems (PVT): technology review and future trends. Renew Sustain Energy Rev 2018;92:848–82. https://doi.org/10.1016/j.rser.2018.04.067.
[21] Herrando M, Pantaleo AM, Wang K, Markides CN. Solar combined cooling, heating and power systems based on hybrid PVT, PV or solar-thermal collectors for building applications. Renew Energy 2019;143:637–47. https://doi.org/10.1016/j.renene.2019.05.004.
[22] Herrando M, Coca-Ortegón A, Guedea I, Fueyo N. Solar assisted heat pump systems based on hybrid PVT collectors for the provision of hot water, cooling and electricity in buildings. ISES Conf. Proc. - Eurosun 2020:2020.
[23] Mittelman G, Kribus A, Dayan A. Solar cooling with concentrating photovoltaic/thermal (CPVT) systems. Energy Convers Manag 2007;48:2481–90. https://doi.org/10.1016/J.ENCONMAN.2007.04.004.
[24] Calise F, Dentice d'Accadia M, Palombo A, Vanoli L. Dynamic simulation of a novel high-temperature solar trigeneration system based on concentrating photovoltaic/thermal collectors. Energy 2013;61:72–86. https://doi.org/10.1016/j.energy.2012.10.008.
[25] Buonomano A, Calise F, Palombo A. Solar heating and cooling systems by CPVT and ET solar collectors: a novel transient simulation model. Appl Energy 2013;103:588–606. https://doi.org/10.1016/J.APENERGY.2012.10.023.
[26] Xu Z, Kleinstreuer C. Concentration photovoltaic–thermal energy co-generation system using nanofluids for cooling and heating. Energy Convers Manag 2014;87:504–12. https://doi.org/10.1016/J.ENCONMAN.2014.07.047.
[27] Buonomano A, Calise F, Palombo A. Solar heating and cooling systems by absorption and adsorption chillers driven by stationary and concentrating photovoltaic/thermal solar collectors: modelling and simulation. Renew Sustain Energy Rev 2018;82:1874–908. https://doi.org/10.1016/j.rser.2017.10.059.
[28] Chen H, Li Z, Xu Y. Evaluation and comparison of solar trigeneration systems based on photovoltaic thermal collectors for subtropical climates. Energy Convers Manag 2019;199:111959. https://doi.org/10.1016/j.enconman.2019.111959.
[29] Herrando M, Ramos A, Zabalza I, Markides CN. Energy performance of a solar trigeneration system based on a novel hybrid PVT panel for residential applications. ISES Sol. World Congr 2017:1090–101. 2017, Proc., Abu Dhabi (UAE) 2017 - IEA SHC int. Conf. Sol. Heat. Cool. Build. Ind.
[30] Herrando M, Simón R, Guedea I, Fueyo N. The challenges of solar hybrid PVT systems in the food processing industry. Appl Therm Eng 2020:116235. https://doi.org/10.1016/j.applthermaleng.2020.116235.
[31] Calise F, Dentice D'Accadia M, Vanoli L. Design and dynamic simulation of a novel solar trigeneration system based on hybrid photovoltaic/thermal collectors (PVT). Energy Convers Manag 2012;60:214–25. https://doi.org/10.1016/j.enconman.2012.01.025.
[32] Ramos A, Chatzopoulou MA, Guarracino I, Freeman J, Markides CN. Hybrid photovoltaic-thermal solar systems for combined heating, cooling and power provision in the urban environment. Energy Convers Manag 2017;150:838–50. https://doi.org/10.1016/j.enconman.2017.03.024.
[33] Vaishak S, Bhale PV. Photovoltaic/thermal-solar assisted heat pump system: current status and future prospects. Sol Energy 2019;189:268–84. https://doi.org/10.1016/j.solener.2019.07.051.
[34] Michael JJ, Iniyan S, Goic R. Flat plate solar photovoltaic-thermal (PV/T) systems: a reference guide. Renew Sustain Energy Rev 2015;51:62–88. https://doi.org/10.1016/j.rser.2015.06.022.
[35] Kamel RS, Fung AS. Modeling, simulation and feasibility analysis of residential BIPV/T+ASHP system in cold climate—Canada. Energy Build 2014;82:758–70. https://doi.org/10.1016/j.enbuild.2014.07.081.
[36] Choi HU, Kim YB, Son CH, Yoon JI, Choi KH. Experimental study on the performance of heat pump water heating system coupled with air type PV/T collector. Appl Therm Eng 2020;178:115427. https://doi.org/10.1016/j.applthermaleng.2020.115427.
[37] Kamthania D, Nayak S, Tiwari GN. Performance evaluation of a hybrid photovoltaic thermal double pass facade for space heating. Energy Build 2011;43:2274–81. https://doi.org/10.1016/j.enbuild.2011.05.007.
[38] Choi H-U, Kim Y-B, Son C-H, Yoon J-I, Choi K-H. Experimental study on the performance of heat pump water heating system coupled with air type PV/T collector. Appl Therm Eng 2020;178:115427. https://doi.org/10.1016/j.applthermaleng.2020.115427.
[39] Kamel RS, Fung AS, Dash PRH. Solar systems and their integration with heat pumps: a review. Energy Build 2015;87:395–412. https://doi.org/10.1016/j.enbuild.2014.11.030.
[40] Ji J, Keliang L, Chow TT, Pei G, Wei H, Hanfeng H. Performance analysis of a photovoltaic heat pump. Appl Energy 2008;85:680–93. https://doi.org/10.1016/j.apenergy.2008.01.003.
[41] de Keizer C, Bottse J, De Jong M. PVT Benchmark. An overview of PVT modules on the European market and the barriers and opportunities for the Dutch Market. 2017.
[42] Fang G, Hu H, Liu X. Experimental investigation on the photovoltaic-thermal solar heat pump air-conditioning system on water-heating mode. Exp Therm Fluid Sci 2010;34:736–43. https://doi.org/10.1016/j.expthermflusci.2010.01.002.
[43] Obalanlege MA, Mahmoudi Y, Douglas R, Ebrahimnia-Bajestan E, Davidson J, Bailie D. Performance assessment of a hybrid photovoltaic-thermal and heat pump system for solar heating and electricity. Renew Energy 2020;148:558–72. https://doi.org/10.1016/j.renene.2019.10.061.
[44] Zhao X, Zhang X, Riffat SB, Su Y. Theoretical study of the performance of a novel PV/e roof module for heat pump operation. Energy Convers Manag 2011;52:603–14. https://doi.org/10.1016/j.enconman.2010.07.036.
[45] Chow TT, Fong KF, Pei G, Ji J, He M. Potential use of photovoltaic-integrated solar heat pump system in Hong Kong. Appl Therm Eng 2010;30:1066–72. https://doi.org/10.1016/j.applthermaleng.2010.01.013.
[46] Keliang L, Ji J, Tin-tai C, Pei G, Hanfeng H, Aiguo J, et al. Performance study of a photovoltaic solar assisted heat pump with variable-frequency compressor – a case

study in Tibet. Renew Energy 2009;34:2680–7. https://doi.org/10.1016/j.renene.2009.04.031.
[47] Xu G, Deng S, Zhang X, Yang L, Zhang Y. Simulation of a photovoltaic/thermal heat pump system having a modified collector/evaporator. Sol Energy 2009;83:1967–76. https://doi.org/10.1016/j.solener.2009.07.008.
[48] Braun R, Haag M, Stave J, Abdelnour N, Eicker U. System design and feasibility of trigeneration systems with hybrid photovoltaic-thermal (PVT) collectors for zero energy office buildings in different climates. Sol Energy 2020;196:39–48. https://doi.org/10.1016/j.solener.2019.12.005.
[49] Mohanraj M, Belyayev Y, Jayaraj S, Kaltayev A. Research and developments on solar assisted compression heat pump systems – a comprehensive review (Part-B: applications). Renew Sustain Energy Rev 2018;83:124–55. https://doi.org/10.1016/J.RSER.2017.08.086.
[50] Ji J, Hanfeng H, Chow T, Pei G, He W, Liu K. Distributed dynamic modeling and experimental study of PV evaporator in a PV/T solar-assisted heat pump. Int J Heat Mass Tran 2009;52:1365–73. https://doi.org/10.1016/j.ijheatmasstransfer.2008.08.017.
[51] Vaishak S, Bhale PV. Performance analysis of a heat pump-based photovoltaic/thermal (PV/T) system. Clean Technol Environ Policy 2020. https://doi.org/10.1007/s10098-020-01839-6.
[52] Chen H, Riffat SB, Fu Y. Experimental study on a hybrid photovoltaic/heat pump system. Appl Therm Eng 2011;31:4132–8. https://doi.org/10.1016/j.applthermaleng.2011.08.027.
[53] Zhou C, Liang R, Riaz A, Zhang J, Chen J. Experimental investigation on the trigeneration performance of roll-bond photovoltaic thermal heat pump system during summer. Energy Convers Manag 2019;184:91–106. https://doi.org/10.1016/j.enconman.2018.12.028.
[54] Zhou C, Liang R, Zhang J, Riaz A. Experimental study on the cogeneration performance of roll-bond-PVT heat pump system with single stage compression during summer. Appl Therm Eng 2019;149:249–61. https://doi.org/10.1016/j.applthermaleng.2018.11.120.
[55] Liang R, Zhou C, Zhang J, Chen J, Riaz A. Characteristics analysis of the photovoltaic thermal heat pump system on refrigeration mode: an experimental investigation. Renew Energy 2020;146:2450–61. https://doi.org/10.1016/j.renene.2019.08.045.
[56] Zhou J, Zhao X, Ma X, Qiu Z, Ji J, Du Z, et al. Experimental investigation of a solar driven direct-expansion heat pump system employing the novel PV/micro-channels-evaporator modules. Appl Energy 2016;178:484–95. https://doi.org/10.1016/j.apenergy.2016.06.063.
[57] Cui Y, Zhu J, Zoras S, Qiao Y, Zhang X. Energy performance and life cycle cost assessments of a photovoltaic/thermal assisted heat pump system. Energy 2020;206:118108. https://doi.org/10.1016/j.energy.2020.118108.
[58] Liang R, Pan Q, Wang P, Zhang J. Experiment research of solar PV/T cogeneration system on the building façade driven by a refrigerant pump. Energy 2018;161:744–52. https://doi.org/10.1016/j.energy.2018.07.189.
[59] Zhang X, Zhao X, Xu J, Yu X. Characterization of a solar photovoltaic/loop-heat-pipe heat pump water heating system. Appl Energy 2013;102:1229–45. https://doi.org/10.1016/j.apenergy.2012.06.039.
[60] Zhang X, Shen J, Xu P, Zhao X, Xu Y. Socio-economic performance of a novel solar photovoltaic/loop-heat-pipe heat pump water heating system in three different climatic regions. Appl Energy 2014;135:20–34. https://doi.org/10.1016/j.apenergy.2014.08.074.
[61] Calise F, Figaj RD, Vanoli L. A novel polygeneration system integrating photovoltaic/thermal collectors, solar assisted heat pump, adsorption chiller and electrical energy storage: dynamic and energy-economic analysis. Energy Convers Manag 2017;149:798–814. https://doi.org/10.1016/J.ENCONMAN.2017.03.027.
[62] Kong R, Deethayat T, Asanakham A, Kiatsiriroat T. Performance and economic evaluation of a photovoltaic/thermal (PV/T)-cascade heat pump for combined cooling, heat and power in tropical climate area. J Energy Storage 2020;30:101507. https://doi.org/10.1016/j.est.2020.101507.
[63] Dannemand M, Sifnaios I, Tian Z, Furbo S. Simulation and optimization of a hybrid unglazed solar photovoltaic-thermal collector and heat pump system with two storage tanks. Energy Convers Manag 2020;206:112429. https://doi.org/10.1016/j.enconman.2019.112429.
[64] Calise F, Dentice d'Accadia M, Figaj RD, Vanoli L. Thermoeconomic optimization of a solar-assisted heat pump based on transient simulations and computer Design of Experiments. Energy Convers Manag 2016;125:166–84. https://doi.org/10.1016/J.ENCONMAN.2016.03.063.
[65] Ma J, Fung AS, Brands M, Abul Moyeed OM, Mhanna A, Juan N. Effects of photovoltaic/thermal (PV/T) control strategies on the performance of liquid-based PV/T assisted heat pump for space heating. Renew Energy 2021;172:753–64. https://doi.org/10.1016/j.renene.2021.02.030.
[66] Calise F, Dentice d'Accadia M, Figaj RD, Vanoli L. A novel solar-assisted heat pump driven by photovoltaic/thermal collectors: dynamic simulation and thermoeconomic optimization. Energy 2016;95:346–66. https://doi.org/10.1016/J.ENERGY.2015.11.071.
[67] Wang G, Zhao Y, Quan Z, Tong J. Application of a multi-function solar-heat pump system in residential buildings. Appl Therm Eng 2018;130:922–37. https://doi.org/10.1016/j.applthermaleng.2017.10.046.
[68] Wang G, Quan Z, Zhao Y, Sun C, Deng Y, Tong J. Experimental study on a novel PV/T air dual-heat-source composite heat pump hot water system. Energy Build 2015;108:175–84. https://doi.org/10.1016/j.enbuild.2015.08.016.
[69] Zhou J, Zhao X, Ma X, Du Z, Fan Y, Cheng Y, et al. Clear-days operational performance of a hybrid experimental space heating system employing the novel mini-channel solar thermal & PV/T panels and a heat pump. Sol Energy 2017;155:464–77. https://doi.org/10.1016/j.solener.2017.06.056.
[70] Bai Y, Chow TT, Ménézo C, Dupeyrat P. Analysis of a hybrid PV/thermal solar-assisted heat pump system for sports center water heating application. Int J Photoenergy 2012;2012. https://doi.org/10.1155/2012/265838.
[71] Dannemand M, Perers B, Furbo S. Performance of a demonstration solar PVT assisted heat pump system with cold buffer storage and domestic hot water storage tanks. Energy Build 2019;188–189:46–57. https://doi.org/10.1016/j.enbuild.2018.12.042.
[72] Croci L, Molinaroli L, Quaglia P. Dual source solar assisted heat pump model development, validation and comparison to conventional systems. Energy Proc 2017;140:408–22. https://doi.org/10.1016/J.EGYPRO.2017.11.153.
[73] Bellos E, Tzivanidis C, Moschos K, Antonopoulos KA. Energetic and financial evaluation of solar assisted heat pump space heating systems. Energy Convers Manag 2016;120:306–19. https://doi.org/10.1016/J.ENCONMAN.2016.05.004.
[74] Cai J, Ji J, Wang Y, Zhou F, Yu B. A novel PV/T-air dual source heat pump water heater system: dynamic simulation and performance characterization. Energy Convers Manag 2017;148:635–45. https://doi.org/10.1016/J.ENCONMAN.2017.06.036.
[75] Wang X, Xia L, Bales C, Zhang X, Copertaro B, Pan S, et al. A systematic review of recent air source heat pump (ASHP) systems assisted by solar thermal, photovoltaic and photovoltaic/thermal sources. Renew Energy 2020;146:2472–87. https://doi.org/10.1016/j.renene.2019.08.096.
[76] Herrando M, Markides CN. Hybrid PV and solar-thermal systems for domestic heat and power provision in the UK: techno-economic considerations. Appl Energy 2016;161:512–32. https://doi.org/10.1016/j.apenergy.2015.09.025.
[77] Baggenstos A, Mellor A, Gagliano A, Corino C, Zenhäusern D, Cabral D, et al. Existing PVT systems and solutions. IEA SHC Task60, PVT Systems, Report A1 2020:130. doi:10.18777/ieashc-task60-2020-0001.
[78] International Energy Agency. (IEA),Task 60: Application of PVT Collectors and New Solutions in HVAC Systems. Solar Heating and Cooling (SHC) programme. https://task60.iea-shc.org/.
[79] Mohanraj M, Belyayev Y, Jayaraj S, Kaltayev A. Research and developments on solar assisted compression heat pump systems – a comprehensive review (Part A: modeling and modifications). Renew Sustain Energy Rev 2018;83:90–123. https://doi.org/10.1016/J.RSER.2017.08.022.
[80] Hu M, Zhao B, Ao X, Ren X, Cao J, Wang Q, et al. Performance assessment of a trifunctional system integrating solar PV, solar thermal, and radiative sky cooling. Appl Energy 2020;260:114167. https://doi.org/10.1016/j.apenergy.2019.114167.
[81] Herrando M, Elduque D, Javierre C, Fueyo N. Life Cycle Assessment of solar energy systems for the provision of heating, cooling and electricity in buildings: a comparative analysis. Energy Convers Manag 2022;257:115402. https://doi.org/10.1016/j.enconman.2022.115402.
[82] Akmese S, Omeroglu G, Comakli O. Photovoltaic thermal (PV/T) system assisted heat pump utilization for milk pasteurization. Sol Energy 2021;218:35–47. https://doi.org/10.1016/j.solener.2021.02.014.
[83] Jia Y, Alva G, Fang G. Development and applications of photovoltaic–thermal systems: a review. Renew Sustain Energy Rev 2019;102:249–65. https://doi.org/10.1016/j.rser.2018.12.030.
[84] Brahim T, Jemni A. Economical assessment and applications of photovoltaic/thermal hybrid solar technology: a review. Sol Energy 2017;153:540–61. https://doi.org/10.1016/j.solener.2017.05.081.
[85] Gürlich D, Dalibard A, Eicker U. Photovoltaic-thermal hybrid collector performance for direct trigeneration in a European building retrofit case study. Energy Build 2017;152:701–17. https://doi.org/10.1016/j.enbuild.2017.07.081.
[86] Gobierno de España, Orden FOM/1635/2013, de 10 de septiembre, por la que se actualiza el Documento Básico DB-HE «Ahorro de Energía», del Código Técnico de la Edificación, aprobado por Real Decreto 314/2006, de 17 de marzo. 2013.
[87] Coca-ortegón A, Herrando M, Simón-allué R, Fueyo N. Experimental study of a heating and cooling pilot installation driven by a hybrid PV-thermal solar field. ISES Conf. Proc. - SWC 2021;2021.
[88] Endef Solar Solutions. http://endef.com/. [Accessed 15 November 2021].
[89] ISO/TC 180. ISO 9806:2017 - solar energy — solar thermal collectors — test methods. 2017.
[90] Hitachi, YUTAKI S COMBI.https://www.hitachiaircon.es/gamas/aerotermia/yutaki-s-combi. [Accessed 19 July 2021].
[91] Lapesa, GEISER INOX Domestic Hot Water tank. http://www.lapesa.es/en/domestic-hot-water/geiser-inox.html. [Accessed 19 July 2021].
[92] Greenheiss. Greenheiss water storage tank. https://www.greenheiss.com/agua-caliente/interacumuladores. [Accessed 17 December 2021].
[93] Solar Energy Laboratory (SEL). Transient System Simulation Program, TRNSYS 18. TESS -Thermal Energy Systems Specialists. Centre Scientifique et Technique du Bâtiment (CSTB), TESS -Thermal Energy Systems Specialists. University of Wisconsin-Madison 2018. http://www.trnsys.com/.
[94] Florschuetz LW. Extension of the Hottel-Whillier model to the analysis of combined photovoltaic/thermal flat plate collectors. Sol Energy 1979;22:361–6. https://doi.org/10.1016/0038-092X(79)90190-7.
[95] Drück H. MULTIPORT Store - Model for TRNSYS 2006:2–27.
[96] Ibrahim A, Othman MY, Ruslan MH, Alghoul MA, Yahya M, Zaharim A, et al. Performance of photovoltaic thermal collector (PVT) with different absorbers design. WSEAS Trans Environ Dev 2009;5:321–30.
[97] Kalogirou SA, Tripanagnostopoulos Y. Hybrid PV/T solar systems for domestic hot water and electricity production. Energy Convers Manag 2006;47:3368–82. https://doi.org/10.1016/j.enconman.2006.01.012.
[98] Simón-Allué R, Guedea I, Coca-Ortegón A, Villén R, Brun G. Performance evaluation of PVT panel with phase change material: experimental study in lab testing and field measurement. Sol Energy 2022;241:738–51. https://doi.org/10.1016/j.solener.2022.05.035.